Construction and Building Materials 320 (2022) 126280

Contents lists available at ScienceDirect

Construction and Building Materials

journal homepage: www.elsevier.com/locate/conbuildmat

Validation of slag-binder fiber-reinforced self-compacting concrete with slag aggregate under field conditions: Durability and real strength development

Vanesa Ortega-López [a,b,*], Flora Faleschini [b], Carlo Pellegrino [b], Víctor Revilla-Cuesta [a], Juan M. Manso [a]

[a] Department of Civil Engineering, Escuela Politécnica Superior, University of Burgos, c/ Villadiego s/n, 09001 Burgos, Spain
[b] Department of Civil, Environmental and Architectural Engineering (ICEA), University of Padova, via Francesco Marzolo 9, 35131 Padova, Italy

ARTICLE INFO

Keywords:
Ground granulated blast furnace slag
Electric arc furnace slag
Fiber-reinforced self-compacting concrete
Core drilling
Real strength development
Durability performance
External aggressive agents

ABSTRACT

The environmental conditions to which a concrete may be exposed will condition its real range of use. Thus, concrete behavior must, at all times, be verified under a wide variety of environmental conditions, in order to ensure its real applicability. In this study, the real strength development and durability behavior of a fiber-reinforced self-compacting concrete is analyzed. This particular concrete incorporates 100% coarse (4/12 mm) and fine (0/4 mm) Electric Arc Furnace Slag (EAFS) as aggregate, as well as limestone fines as aggregate powder (0/1.18 mm). Furthermore, Ground Granulated Blast Furnace Slag (GGBFS) was also added as binder. Four mixtures with and without either metallic or synthetic fibers, and different GGBFS contents were designed. Real strength development was evaluated in all the mixes by comparing the strength development of both cores extracted from full-scale beams and wet-cured laboratory specimens. The durability behavior was analyzed by Mercury Intrusion Porosimetry (MIP), freeze/thaw, moist/dry, sulfate-attack, chloride-penetration, carbonation, and SO_2-attack tests. On the one hand, the long-term mechanical properties of the cores (real conditions) were similar to the properties of the specimens cured in a moist chamber for 90 days in all the mixes. On the other, the increase in water content when adding fibers to maintain flowability, as well as the addition of GGBFS, resulted in an increase in MIP porosity. Therefore, the use of fibers, both metallic and synthetic, slightly worsened the durability behavior of the concrete, facilitating the entry of aggressive external agents. Nevertheless, the increased flexibility of the cementitious matrix when adding GGBFS was beneficial against moist/dry and sulfate-attack phenomena, despite the increase in porosity. Overall, the mixes complied with the regulatory requirements for use in aggressive environments, although the amounts of fibers and GGBFS should be carefully studied.

1. Introduction

Self-Compacting Concrete (SCC) is a type of concrete that was first developed between the end of the 20th century and the beginning of the 21st century through the research work of Okamura and Ouchi [1,2]. They discovered that if concrete was designed with certain particularities in its composition, the vibration phase could be eliminated during its placement [1]. These design features are essentially threefold. First, the aggregate should have a high content of fine particles smaller than 0.063 mm in terms of its overall granulometry [3], which is intended to create a sufficiently compact cement paste that will successfully drag the larger aggregate particles [4]. Second, the amount of coarse aggregate to be added should be less than the amount of fine aggregate [5], so that all aggregate particles may be uniformly dragged within the cement paste [6]. Finally, it is necessary to use a plasticizer or superplasticizer admixture for a cement paste with high flowability and low viscosity

Abbreviations: EAFS, electric arc furnace slag; GGBFS, ground granulated blast furnace slag; MIP, mercury intrusion porosimetry; SCC, self-compacting concrete; UPV, ultrasonic pulse velocity.

* Corresponding author at: Department of Civil Engineering, University of Burgos, Escuela Politécnica Superior, c/ Villadiego s/n, 09001 Burgos, Spain.
E-mail addresses: vortega@ubu.es (V. Ortega-López), flora.faleschini@dicea.unipd.it (F. Faleschini), carlo.pellegrino@unipd.it (C. Pellegrino), vrevilla@ubu.es (V. Revilla-Cuesta), jmmanso@ubu.es (J.M. Manso).

https://doi.org/10.1016/j.conbuildmat.2021.126280
Received 20 September 2021; Received in revised form 23 November 2021; Accepted 28 December 2021
Available online 8 January 2022

[7,8].

Despite its complex composition, the absence of vibration in SCC makes it a very desirable type of concrete for two main reasons. On the one hand, it can be pumped on site at any location and into any formwork shape. Thus, SCC is an optimal type of concrete for any structural application [9]. On the other hand, its energy savings result in a smaller carbon footprint and, in turn, an increase in the sustainability of the construction sector [10].

The use of concrete reinforced with both metallic and synthetic fibers is also a trend that is currently spreading [11–13]. Their use significantly constrains concrete workability [14], although their advantages in the hardened state are notable. On the one hand, they provide high post-cracking strength, increasing the safety of any in-service structure in the event of a possible collapse [11,15]. In addition, they increase the tensile and flexural strength of concrete, as well as its impact resistance, thanks to their crack bridging [16]. This reduction in concrete cracking usually also ensures improved durable behavior by reducing the potential penetration of damaging external agents into concrete, which corrode the reinforcements [17]. The use of fibers in SCC also has these advantages in the hardened state, although fibers are an obstacle to achieving optimum self-compactability [18] and usually hinder the uniform dragging of the larger aggregate particles. Therefore, the definition of an adequate proportion of fibers is essential to produce a fiber-reinforced concrete that can be placed without vibration [14].

One common strategy to reduce the environmental impact of the construction sector is to use waste or industrial by-products as raw materials in concrete production [19–21]. The substitution of natural aggregate for Electric Arc Furnace Slag (EAFS) is a widespread practice [22]. This industrial by-product is obtained during the manufacture of steel from scrap iron in electric arc furnaces, and its annual production in Europe alone is around 8 Mt [23]. It is characterized by its black color, high density of around 3.5 Mg/m^3 and high roughness and microporosity [22]. It adds adequate strength, stiffness and durability to cementitious mixes, in addition to increasing their sustainability indices [24]. Moreover, its high density is very useful when heavy concrete elements are needed, such as foundations, and sea-wall breakwater blocks and tetrapods [25]. However, an EAFS concrete with adequate workability must first be produced to achieve these hardened-state benefits [26]. The high weight of EAFS hinders adequate dragging within the concrete matrix, fresh-performance problems that are amplified in SCC, in which it is even necessary to conduct numerical simulations for a successful design [5]. The few existing studies of SCC with EAFS show that its structural and durability behavior is optimal for its use, but the mix design has to be very careful to ensure self-compactability [27].

The aforementioned efforts to promote sustainability in the field of concrete are now also being extended to the field of binders [28–30]. Therefore, waste or industrial by-products are not only being used as substitutes for aggregates, but also for ordinary Portland cement [31]. The reason is clear: for every ton of Portland cement produced, approximately one ton of CO_2 is emitted into the atmosphere [32]. One standard alternative binder is Ground Granulated Blast Furnace Slag (GGBFS), which is produced from the sudden cooling and grounding of blast furnace slag [31]. Around 22 Mt of GGBFS, which has pozzolanic properties, are annually produced in Europe alone [23]. The lower mechanical strength provided by this binder compared to Portland cement has meant that it has traditionally been used for soil stabilization [33] and in the construction of submerged concrete structures not subjected to very high stresses [34]. In fact, some standardized cements (EN 197-1 [35]) used in these applications, such as CEM III and some types of CEM II, incorporate GGBFS in their composition. However, recent research has shown that, if the amount of binder is adapted to compensate for the expected loss of strength, then the partial replacement of conventional cement with GGBFS will yield concretes of adequate structural strength and durability [36]. Furthermore, proper adjustment of the proportion of coarse aggregate in concrete is needed, due to the high grinding fineness of this binder, which reduces the dragging capacity of the cement paste in the fresh state [37]. Therefore, manufacturing SCC with this alternative binder has an additional difficulty, since a binder with a reduced aggregate-dragging capacity is used, which is a fundamental property in the fresh performance of SCC [38].

In summary, the separate use of fibers, EAFS and GGBFS in SCC has advantages for strength and durability performance, as well as for increasing concrete sustainability. However, the design has to be carefully performed to ensure adequate self-compactability. Accordingly, the aim of this paper, the main novelty of this research work, is to describe the composition of an SCC made with all the above-mentioned raw materials, such that the concrete designed could be called a slag-binder EAFS-aggregate fiber-reinforced self-compacting concrete. Both metallic and synthetic fibers were considered in the development of SCC, to provide a detailed analysis of the effect of fibers and their interaction with EAFS. In addition, an extensive validation of the use of these concretes under conditions similar to those found in a real concrete structure was conducted, which is also a novel aspect in the literature. So, its strength development under field conditions (large volume of concrete used to manufacture full-scale structures) was analyzed by core drilling and its durability behavior was evaluated under different environmental conditions (freeze/thaw, moist/dry, attack by sulfates, chlorides, and SO_2, and carbonation).

2. Materials and methods

2.1. Materials

2.1.1. Binders, water and admixtures

Two different cements according to EN 197-1 [35] were used: CEM II/B-S 42.5 N and CEM III/B 32.5 N. These two cements were characterized by a GGBFS content of around 30% and 70%, respectively, and a specific weight of approximately 3 Mg/m^3. CEM II/B-S was used in a first phase of the research, in which SCC was successfully developed. CEM III/B was used in a second phase to study the feasibility of doubling the GGBFS content when producing fiber-reinforced SCC with EAFS.

Mix water was obtained from the mains water supply. Its use was adequate for the production of concrete according to previous experience of the authors [38,39].

A carboxylate-based admixture, which acted simultaneously as a plasticizer and viscosity conditioner, was used to reach adequate self-compactability. Its main characteristic was a good interaction with EAFS, as shown in other studies by the authors [55,39].

2.1.2. Aggregates

EAFS was used for all the coarse (4/12 mm) and fine (0/4 mm) aggregate of the mixes. This aggregate was supplied previously separated into fractions by a company exclusively dedicated to the management of this type of waste. It was characterized by a high density (3.42 Mg/m^3), a medium 24-h water absorption (1.12%) and an irregular shape (angularity coefficient as per BS-812 [40] around of 11 units). The results of the X-ray fluorescence analysis of the EAFS performed by the authors are listed in Table 1. They show the typical chemical composition of EAFS, characterized by the predominance of calcium and iron oxides. The gradation of the EAFS is depicted in Fig. 1, in which a continuous grading optimal for concrete production can be noted. The fineness moduli of the coarse and fine fractions were 5.7 and 3.9 units, respectively. The slag was exposed for three months to the outdoor environment for spontaneous wetting and correct dimensional stabilization before use, thus simulating the usual practice in real works executed with EAFS concrete, which has yielded good results [25].

As indicated in the introduction, a high proportion of particles smaller than 0.063 mm is required to obtain SCC [1]. EAFS is characterized by a low content of particles of this size, which also tend to have a very irregular shape [41]. Limestone fines 0/1.18 mm were therefore added as aggregate powder to provide the SCC mixes with aggregate particles of that size. This aggregate had a calcite content of over 95%, a

Table 1
X-ray fluorescence analysis of EAFS (chemical composition).

CaO	Fe_2O_3	SiO_2	Al_2O_3	MnO	MgO	Cr_2O_3	TiO_2	SO_3	P_2O_5	Others (Na_2O…)
32.9	22.3	20.4	12.1	5.0	3.0	2.0	0.8	0.4	0.5	0.6

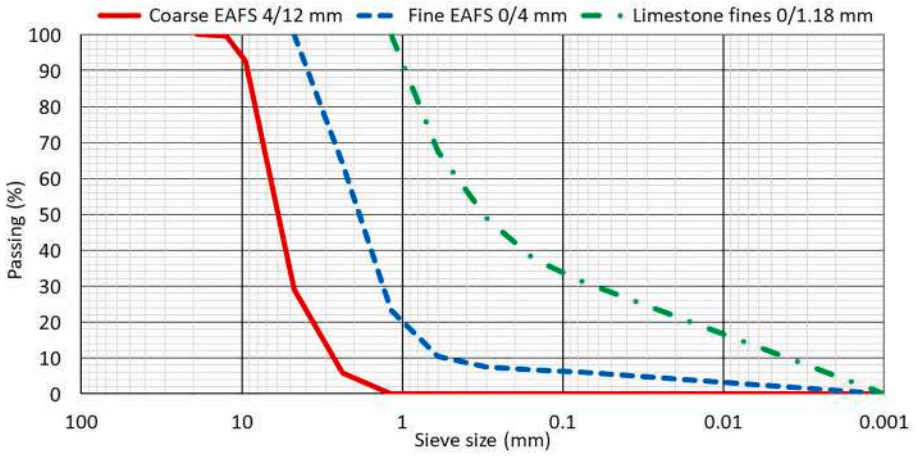

Fig. 1. Particle gradation of the aggregates.

density of 2.65 Mg/m^3 and a 24-h water absorption of 0.53%. Its particle gradation (fineness modulus of 1.5 units) is also shown in Fig. 1.

2.1.3. Fibers

Non-recycled metallic and synthetic fibers were used, which were added separately to the SCC. Both fiber types were supplied by SIKA. The metallic fibers were hooked-end wire pieces of steel, while the synthetic fibers were surface-dimpled polypropylene pieces. These surface and shape characteristics ensured good adhesion between the fibers and the cementitious matrix [42]. Table 2 shows the characteristics of the fibers in detail.

2.2. Mix design

In this research work, the behavior of four different mixes made with or without metallic or synthetic fibers was studied:

- First, the "reference mix" without fibers was designed according to the guidelines of previous works by the authors [55,39]. These guidelines were an adequate adjustment of the overall aggregate particle size to the Fuller curve with an exponent of 0.45, a water-to-binder ratio of around 0.5 units, and a cement content of around 320–330 kg/m^3, to achieve a 28-day compressive strength between 30 and 50 MPa in specimens conserved in a moist chamber. This mix incorporated, in addition to CEM II/B-S, 100% EAFS in the coarse and fine aggregate fractions. Limestone fines 0/1.18 mm were also added to achieve self-compactability (slump flow of around 700 mm). Previous studies of this research group have analyzed the use of EAFS instead of natural aggregate in SCC and its effects on durability [43,44]. In this research work, the aim was to analyze the interaction of EAFS with fibers, which explains why the EAFS content of the SCC mixes was maximized in relation to the reference mix.
- Subsequently, two fiber-reinforced SCC mixes were designed, one with metallic fibers and the other with synthetic fibers. These mixtures had exactly the same composition as the reference mix, but fibers were added and the water content was adjusted to ensure self-compactability. The fiber content, which was empirically determined from previous mixtures to adjust the mix design, was 0.5% by concrete volume, regardless of the fiber type. This content was the maximum possible to reach self-compactability without excessively increasing the water content.
- Finally, it was decided to design a mix with exactly the same composition as the metallic-fiber-reinforced mix, but using CEM III/B (70% GGBFS). However, poor interaction between the GGBFS and the admixture, which should not exceed 2% of the cement mass to avoid segregation, according to previous experience [55,39], resulted in an inadequate flow of the cement paste. The cement paste was unable to drag the larger EAFS particles, and self-compactability could not be reached. The problems persisted, even though the EAFS and limestone fines contents were readjusted. In view of that situation, it was decided to develop a concrete of high workability (pumpable concrete of slump class S4, slump between 160 and 210 mm, EN 206 [35]) by maximizing the EAFS content (adjustment of the proportion of the different aggregates) and using CEM III/B. The objective was to study the behavior of a cementitious matrix with a high proportion of GGBFS in a concrete made with both EAFS and fibers. Therefore, the introduction of this concrete mix in the study is to show that a low-clinker-content concrete that demonstrates high workability and good strength and durability behavior may be obtained, while simultaneously employing three raw materials that hinder the development of a concrete with adequate fresh and hardened performance.

Table 2
Fiber characteristics.

Property	Metallic fibers	Synthetic fibers
Density (kg/m^3)	7900	910
Young's modulus (GPa)	210	6
Tensile strength (MPa)	>1200	>400
Equivalent diameter (mm)	0.55	0.93
Length (mm)	35	35
Aspect ratio	64	38

The composition of the mixes is shown in Table 3, in which all the indicated design aspects can be observed. On the other hand, Fig. 2 shows the global granulometry of both self-compacting and pumpable mixes, where the correct adjustment to the Fuller curve and the adequate content of particles smaller than 0.063 mm of the mixes can be noted. The mixtures were denominated C/B-F:

Table 3
Mix design (kg/m^3).

Mix	CEM II/B-S # CEM III/B	Water	Admixture	Coarse EAFS 4/12 mm # Fine EAFS 0/4 mm	Limestone fines 0/1.18 mm	Fibers
SC/II	325 # 0	170	5.0	755 # 545	955	–
SC/II-M	325 # 0	180	5.0	755 # 545	955	40
SC/II-S	325 # 0	185	5.0	755 # 545	955	4.5
P/III-M	0 # 325	160	4.2	935 # 685	655	40

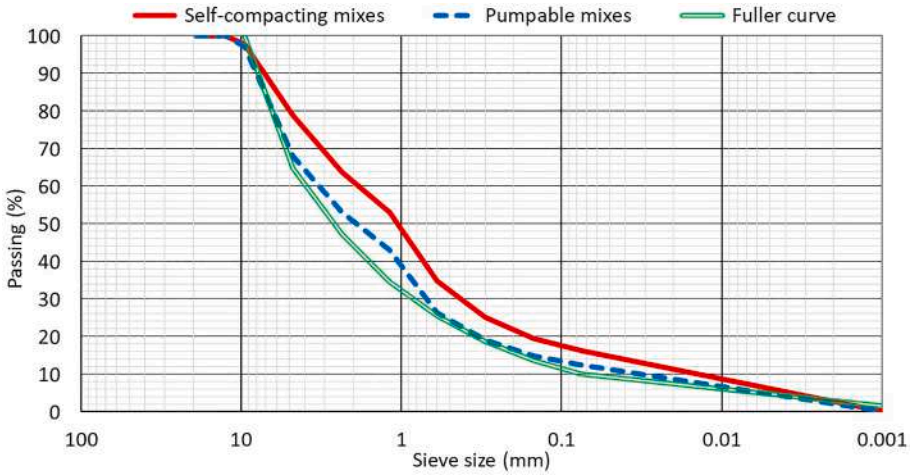

Fig. 2. Joint granulometry of the mixes.

- C: consistency. SC (Self-Compacting mix) or P (Pumpable mix).
- B: type of cement. II (CEM II/B-S) or III (CEM III/B).
- F: fibers. M (Metallic) o S (Synthetic).

2.3. Experimental program

2.3.1. Mixing process and specimen preparation

The mixing process was mechanically performed in four stages with the aim of achieving a homogeneous concrete mix. First, all the aggregates (EAFS and limestone fines) were added and mixed for one minute. Second, the binders and the water were added and mixed for two minutes for adequate hydration of all the components. Third, the admixture was poured in and the whole mixture was mixed for three minutes. At this point, optimum flowability of concrete had to be observed. Finally, the fibers were incorporated, and the SCC was mixed for another minute. The concrete showed adequate homogeneity in all cases, with no segregation of the EAFS from the other components of the mix.

Once the mixing process was completed, the fresh-state tests were performed: slump-flow test (EN 12350-8 [35], SC mixes), slump test (EN 12350-2 [35], mix P/III-M), 3-bar L-box test (EN 12350-10 [35], mix SC/II), fresh-density test (EN 12350-6 [35]) and occluded-air test through the pressure method (EN 12350-7 [35]). These fresh tests were performed using the standardized apparatus described in the referenced standards.

A concrete mass of approximately 0.4 m^3 was prepared for each mix. These masses were then used to produce two 0.2x0.3x4.4-m beams per mix, which were subsequently subjected to various structural tests, the results of which may be found in another work of the authors [45]. The present article shows only unpublished results that aim to validate these concrete mixes in terms of strength development and durability rather than in structural terms. To do so, cores were extracted from the beams to study the real strength development of the mixes. In addition, various types of standardized specimens were prepared at the same time as the beams to ensure full comparability between the concrete used in both the beams and the laboratory specimens. Those laboratory specimens were used to perform the different mechanical and durability tests. In the following sections, the specimens and the tests are presented in precise detail.

2.3.2. Real-strength-development tests

The large concrete volumes composing the real structures, as well as their curing process under ambient conditions (ambient curing), means that their strength development is slightly different from the specimens cured in a moist chamber (wet curing) [46]. The real strength development was therefore studied through cores extracted from the full-scale beams.

After production, the beams were left to cure under ambient conditions in the laboratory for one year so that their strength could stabilize, *i.e.*, so that concrete strength may be considered constant with no increase over time. Subsequently, they were mechanically tested and, exactly one and a half years after their manufacturing, eight 70-mm-diameter cylindrical cores were extracted per beam according to EN 12504-1 [35]. Core drilling was performed at the ends of the beams, between the stirrups, so that the cores were composed exclusively of concrete. Fig. 3 shows the core extraction zones in the beams. Since the width of the beams was 200 mm, the cores were drilled to a slenderness ratio of 2, resulting in 70x140-mm cylindrical cores, which were used for the tests after facing both the top and the bottom ends, to ensure that they were completely flat with no irregularities, as depicted in Fig. 4. Four cores were used to measure compressive strength (EN 12390-3 [35]) and Ultrasonic Pulse Velocity (UPV) (EN 12504-4 [35]). Four other cores were instrumented with strain gauges to determine the modulus of elasticity (EN 12390-13 [35]), as also shown in Fig. 4. The mean values and standard deviations of these mechanical properties were determined using the four test cores of each concrete mix.

On the other hand, six 100x200-mm cylindrical specimens (slenderness 2, results comparable to those of the cores) were prepared for each mix and held in a moist chamber, according to standard requirements, for 90 days. At that moment, the compressive strength and UPV were determined in three of them, while the modulus of elasticity was measured on the other three specimens. The mean values and standard deviations of those mechanical properties were calculated through the results obtained in the three specimens used per test and mix. In this way, the mechanical behaviors of both ambient-cured

Fig. 3. Location of core drilling in the full beams (left) and detail of the ends of the beams (right).

Fig. 4. Faced and instrumented core.

concrete from real structures and wet-cured laboratory specimens were compared. Wet curing of the laboratory specimens means that the mechanical behavior of a real concrete structure can be determined after a little period of time from concreting, due to the quicker strength development of the wet-cured laboratory specimens. Wet-curing is therefore a way of defining the behavior of a real concrete structure within a considerably shorter time.

2.3.3. Durability tests

At the time of concrete production, nineteen 100x100x100-mm cubic specimens were prepared for each mix, as well as two 100x200-mm cylindrical specimens. All of them were used for the durability tests, so that the results of each test for each mixture were always expressed as the mean value and the standard deviation calculated from the values obtained in all the specimens tested for each mix. All these specimens were demolded the day after manufacturing and stored in the indoor environment of the laboratory until the testing moment. The aim was to simulate the ambient curing of concrete in a real structure. The durability tests performed are shown in Table 4, along with the standards and specimens used in each test.

Since each durability test was of a different duration, the starting time of each test was adjusted from eight months after the manufacturing of the test specimens (at that moment the concrete strength could be considered already stabilized [45]), so that they all ended approximately one year after the concrete manufacturing (1 week deviation). At that time, the three cubic specimens not used in the durability tests were tested for hardened density and compressive strength to analyze the loss of density and compressive strength caused by the attack of external agents.

Table 4
Durability tests.

Test	Standard	Number and type of specimens used
Freeze/thaw test	UNE 12390-9-EX [47]	Three 100x100x100-mm cubic specimens
Moist/dry test	ASTM D 559 [48]	Three 100x100x100-mm cubic specimens
Sulfate-attack test	ASTM C 1012 [48]	Three 100x100x100-mm cubic specimens
Chloride-penetration test	EN 12390-11 [35]	Two 100x200-mm cylindrical specimens cut in half
Carbonation (CO_2) test	EN 13295 [35]	Four 100x100x100-mm cubic specimens
SO_2-attack test (Kesternich test)	EN ISO 6988 [35]	Three 100x100x100-mm cubic specimens

The durability behavior is closely dependent on the porosity of concrete, since it conditions the penetration of external agents into it [49]. Consequently, fragments of the specimens stored in a moist chamber and tested for compressive strength at 90 days were subjected to Mercury Intrusion Porosimetry (MIP) tests and their porosity levels were linked to the durability performance.

2.3.4. Overview

Fig. 5 depicts an overview of the experimental program, which shows a chronogram of all the tests described in the previous sections.

3. Results and discussion: fresh behavior

Table 5 shows the fresh properties of the mixes, as well as the different fresh-performance classes according to each test (EN 206 [35]). As indicated in the mix design, the mixes made with CEM II/B-S were self-compacting, with slump-flow classes SF2 without fibers and SF1 with fibers. Mix SC/II also showed adequate passing ability (class PA2). Mix P/III-M showed a slump class S4, implying adequate pumpability.

The results showed that the decrease in filling ability caused by the interposition of the fibers in the flow of the EAFS particles could be partially compensated by the increase in water content. The inadequate ability of GGBFS to drag the EAFS prevented the achievement of self-compactability when CEM III/B was used. However, the slump class ensured that this concrete required only light vibration after on-site pouring [39].

The fresh density of the mixtures was between 2.60 and 2.72 Mg/m^3, higher than that of conventional concrete. The use of EAFS, an aggregate with higher density than natural aggregate, explains this phenomenon [50]. The addition of fibers caused a decrease in the fresh density, due to the required increase in water content; a decrease that was lower in mix SC/II-M, due to the higher density of the metallic fibers.

The occluded air content, which represents the spherical or vacuolar porosity of a concrete mix [38], was around 2% in all the self-compacting mixes. The addition of fibers and the slight modification of the water content hardly affected it. However, the occluded air

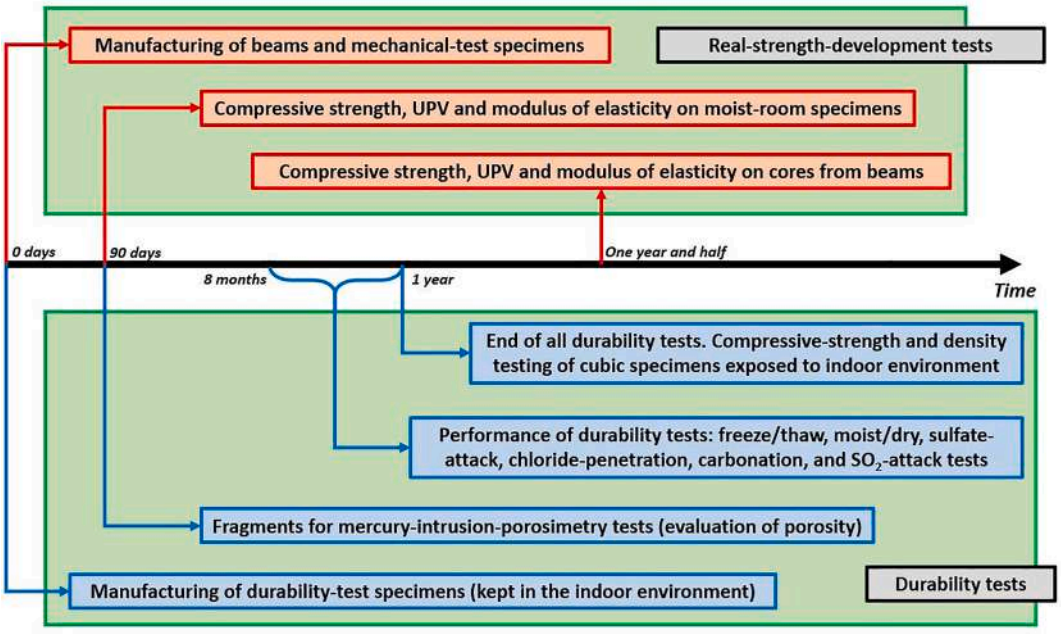

Fig. 5. Overview.

Table 5
Fresh properties.

Mix	Slump flow (mm), EN 12350–8 [35]	Blocking ratio, 3-bar L-box test, EN 12350-10 [35]	Slump (mm), EN 12350-2 [35]	Fresh density (Mg/m^3), EN 12350-6 [35]	Occluded air (%), EN 12350-7 [35]
SC/II	720 (SF2)	0.82 (PA2)	–	2.72	2.3
SC/II-M	650 (SF1)	–	–	2.68	2.1
SC/II-S	620 (SF1)	–	–	2.61	1.8
P/III-M	–	–	175 (S4)	2.72	3.5

content of mix P/III-M reached 3.5%, which is explained by the inadequate interaction between the large GGBFS content of CEM III/B and the admixture.

4. Results and discussion: real strength development

Table 6 shows the results of compressive strength, modulus of elasticity and UPV, both on cores extracted from the beams one and a half years after their manufacturing, and on specimens held in a moist chamber and tested at 90 days. The ratio between the results from both the cores and the specimens is also shown. All the values of compressive strength and modulus of elasticity were adequate for structural use. The addition of fibers reduced the strength by 11–14 MPa, due to the increase in water content required to maintain self-compactability [22]. This phenomenon, not common in conventional concrete, had already been observed in other similar studies [14,16]. Doubling the GGBFS content halved the compressive strength, despite the reduction in water content, due to the lower strength of this alternative binder compared to Portland cement [24]. The trend exhibited by the modulus of elasticity was similar to that of the compressive strength. Finally, the UPV values corresponded to good quality concrete [51].

The compressive strength values of the specimens were slightly higher than those of the cores (around 2%) due to the ambient-curing conditions of the beams for all the mixes. The modulus of elasticity and the UPV, which is closely related to the elastic stiffness of concrete, were between 1% and 6% higher in the cores. No effect of the mix composition was observed on any of the analyzed properties, so neither the addition of fibers nor the amount of GGBFS affected the ratio of the

Table 6
Results of the real-strength-development tests (standard deviation in brackets).

	Cores extracted from beams cured in ambient conditions				Specimens cured during 90 days in moist chamber				Ratio (cores/specimens)			
	SC/II	SC/II-M	SC/II-S	P/III-M	SC/II	SC/II-M	SC/II-S	P/III-M	SC/II	SC/II-M	SC/II-S	P/III-M
Compressive strength (MPa)	74.1 (1.9)	62.7 (1.1)	60.6 (2.4)	32.5 (1.8)	75.3 (4.1)	63.6 (3.6)	61.1 (5.3)	33.3 (1.0)	0.98	0.99	0.99	0.98
Modulus of elasticity (GPa)	42.1 (0.8)	36.0 (0.7)	33.6 (0.4)	26.5 (1.9)	40.1 (0.7)	34.7 (1.5)	31.6 (0.9)	26.1 (0.5)	1.05	1.04	1.06	1.02
UPV (km/s)	4.52 (0.03)	4.29 (0.02)	4.18 (0.06)	4.04 (0.08)	4.45 (0.03)	4.25 (0.08)	4.03 (0.05)	3.84 (0.02)	1.02	1.01	1.04	1.05

values obtained in both cores and specimens.

It can be noted that the results of the specimens stored in a moist chamber for 90 days were similar to those obtained in the long term in an ambient-cured real structure. Thus, accurate long-term estimations of the mechanical behavior of high-workability EAFS concrete with or without fibers under real conditions can be performed by testing specimens stored in a moist chamber for 90 days.

5. Results and discussion: durability

5.1. Preliminary information

5.1.1. Porosity: MIP tests

The higher the porosity of a concrete mix and the greater the interconnectivity between its pores, the worse the durability performance of concrete due to the greater ease of penetration of harmful external agents [44]. To evaluate the porosity of the mixtures, four fragments (size between 2 and 3 cm) of the laboratory specimens tested to compressive strength were selected to measure the porosity through Mercury Intrusion Porosimetry, for which an Autopore IV 9500 apparatus (33,000 psi pressure) was used. Fig. 6 shows the log-differential and cumulative intrusion of the mixtures, while Table 7 shows the porosity of the mixes regarding the mix volume for each pore size.

Table 7
MIP porosity of the mixes (percentage regarding the total volume of the mix, %).

Mix	Pore size < 20 nm	20 nm ≤ Pore size < 50 nm	50 nm ≤ Pore size < 200 nm	Pore size ≥ 200 nm	Total porosity
SC/II	1.1	2.5	3.4	2.5	9.5
SC/II-M	1.3	3.6	3.7	3.7	12.3
SC/II-S	1.4	2.8	4.4	4.8	13.4
P/III-M	4.8	4.4	1.0	4.5	14.7

The total porosity of the mixtures was between 9% and 15%, values slightly higher than those obtained in SCC made with natural aggregate and conventional cement [52]. This is explained by the high microporosity of EAFS [27]. In addition, the use of alternative binders usually also increases the porosity of the cementitious matrix, due to its worse affinity than ordinary Portland cement with the other mix components [53].

In the self-compacting (SC) mixes, total porosity increased with the water content when fibers were added (9.5% for mix SC/II and 12.3%

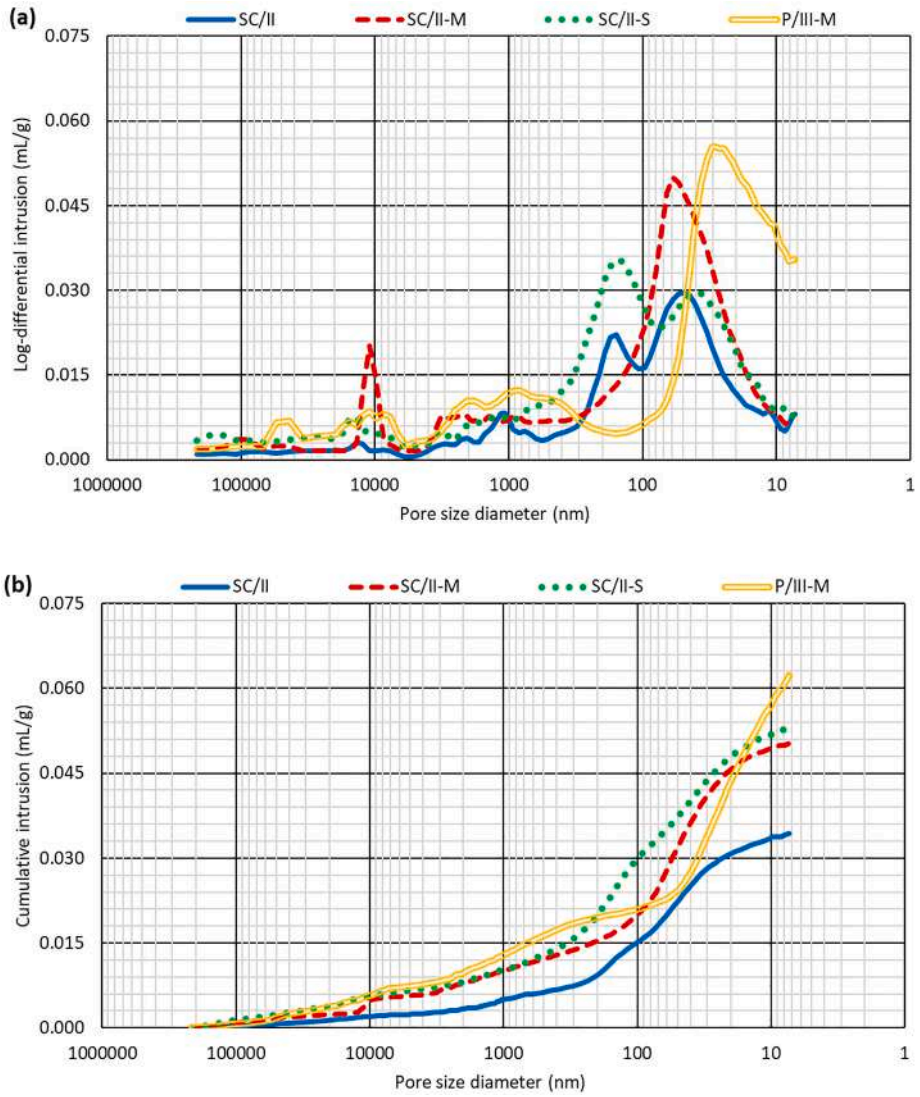

Fig. 6. Results of the MIP tests: (a) log-differential intrusion; (b) cumulative intrusion.

and 13.4% for mixes SC/II-M and SC/II-S, respectively). Thus, the increase in the water-to-binder ratio to compensate for the decrease in flowability (Table 3) caused by the addition of fibers augmented the porosity. The results of porosity were consistent with the compressive strength of the mixes (Table 6), as higher porosity levels meant lower compressive strengths. Thus, mix SC/II achieved a 90-day compressive strength of 74.1 MPa for a porosity of 9.5%. Finally, it should be noted that the highest pore proportions were around 100 nm, a proportion that increased with the addition of fibers and the consequent increment of the water content necessary to maintain the flowability. This pore size is the most favorable for capillary diffusion of water, which shows the dependence of the porosity results on the amount of mix water [3].

Mix P/III-M had the highest porosity (14.7%) despite having the lowest water content. In addition, the largest proportion of pores was less than 100 nm in size, unlike the SC mixes where higher pore sizes were recorded. This phenomenon can be explained on the basis of two aspects. Firstly, the higher EAFS content of this mixture compared to SC mixes. The high micro-porosity of EAFS increased the porosity of the surrounding cementitious matrix [27]. Secondly, the higher specific surface area of the binder, due to the higher fineness of GGBFS than ordinary Portland cement [38], which might favor the appearance of air bubbles of nanometer size during the mixing process (<50 nm).

6. Reference values: hardened density and compressive strength

External aggressive agents that attack concrete can cause compressive strength loss. The compressive strength of concrete undamaged by harmful external agents, *i.e.*, not subjected to durability tests, must be known to evaluate any loss of strength caused by durability processes. That compressive strength can be referred to as the "reference" compressive strength. In principle, compressive strength was measured in 100x200-mm cylindrical specimens held in a moist chamber for 90 days (Table 6), as shown in the analysis of the real strength development. However, in the durability tests, 100x100x100-mm cubic specimens cured in the laboratory under ambient conditions (ambient curing) were used. The compressive strength was measured in ambient-cured 100x100x100-mm cubic specimens, in order to have the reference compressive strength in specimens of the same type cured under the same conditions. The test age was one year after casting, the time at which the durability tests finished. The reference hardened density was also measured on these ambient-cured specimens after 72-h oven-drying, to compare it with the density of the mixtures after durability testing. In this way, the density variation due to durability processes could be determined.

The reference values of hardened density and compressive strength, both calculated as the average of the results of three 100x100x100-mm cubic specimens, are shown in Table 8. The hardened density was in accordance with the fresh density (Table 5): it was high due to the use of EAFS [49] and decreased with the addition of fibers, because of the necessary adjustment of the water content [19]. On the other hand, the same trends as in the moist-chamber cylindrical specimens (Table 6) were also noted for the compressive strengths of the ambient-cured cubic specimens. The only difference was that the cubic specimens yielded values that were slightly higher due to their more compact shape [54].

Table 8
Reference hardened density and compressive strength for durability tests (standard deviation in brackets).

Mix	Reference hardened density (Mg/m^3)	Reference compressive strength on cubic specimens (MPa)
SC/II	2.63 (0.02)	88.3 (2.3)
SC/II-M	2.57 (0.03)	74.3 (2.1)
SC/II-S	2.54 (0.02)	69.0 (1.7)
P/III-M	2.65 (0.04)	47.2 (0.8)

6.1. Freeze/thaw test

The freeze/thaw test was performed as per UNE 12390-9-EX [47], applying the so-called "cube method". Thus, three 100x100x100-mm cubic specimens of each mixture were placed in a stainless-steel container that was subsequently filled with an aqueous solution with 3% by mass of NaCl. The specimens were kept in that way for 24 h, so that they absorbed the solution and the conditions at all their points were homogeneous. Any absorption during this period of time was measured (Table 9). The absorption results of the mixes were in accordance with their porosity (Table 7). Thus, mix SC/II, with the lowest porosity, showed the lowest solution absorption level (0.80%), while the increase in porosity when adding fibers inevitably increased that absorption. The most porous mix, mix P/III-M, had a solution absorption of 3.23%, four times higher than that of mix SC/II. The increases in water absorption in relation to the increments of porosity were in line with those of other EAFS concretes available in the literature [22,43].

Subsequently, the specimens were subjected to 56 freeze/thaw cycles while they remained immersed in the NaCl solution of the container, in a process that simulates extreme winter conditions [55]. Each cycle lasted 24 h and consisted of two stages. In the first stage, the container was placed for 16 h in a freezer whose temperature was adjusted, so that a temperature of -20 ± 1 °C was reached at the center of the specimens. In the second stage, the container was introduced for 8 h in a tank full of water, initially at room temperature, equipped with automatic recirculation and a water temperature control system, to ensure that the center of the specimens reached a temperature of 20 ± 1 °C. The temperature at the central point of the specimens was controlled by a temperature probe inserted in one of the specimens. This probe was positioned after drilling a 6-mm-diameter hole up to the center of the specimen, which was sealed with silicone after the insertion of the probe. At the end of each cycle, the loss of mass of each specimen was measured, with Fig. 7 showing the evolution of the average loss of mass of each mixture throughout the test. Table 9 shows the final mass loss. In addition, the UPV of the specimens was measured every 5 cycles, results that are also shown in Fig. 7 and Table 9. In relation to these aspects, it was noted that:

- Mix SC/II experienced almost no loss of mass during the test (1.75%), as shown in Fig. 7 and Fig. 8b (only a few small flacks on the skin of the specimens). However, mixes SC/II-M and SC/II-S exhibited a practically constant mass loss from the 7th-8th cycle (Fig. 7, approximately constant slopes), the final mass losses amounting to 32.70% and 50.21%, respectively (Table 9). It can therefore be stated that the specimens of these last two mixtures were completely destroyed during the test (Fig. 8c and Fig. 8d). Considering the

Table 9
Results of the freeze/thaw test (standard deviation in brackets).

Mix	SC/II	SC/II-M	SC/II-S	P/III-M
Absorption after 24 h (%)	0.80 (0.12)	1.65 (0.18)	1.90 (0.23)	3.23 (0.31)
Total loss of mass (%)	1.75 (0.23)	32.70 (1.89)	50.21 (3.54)	55.13 (3.78)
Total UPV decrease (%)	15.30 (1.32)	48.93 (2.89)	79.43 (6.54)	84.62 (7.21)
Hardened density after the test (Mg/m^3)	2.60 (0.02)	2.49 (0.02)	2.47 (0.04)	2.61 (0.03)
Average loss of hardened density (%)	1.1 (0.01)	3.1 (0.02)	2.8 (0.01)	1.5 (0.01)
Compressive strength after the test (MPa)	52.2 (2.3)	–	–	–
Average loss of compressive strength (%)	40.94 (2.85)	–	–	–

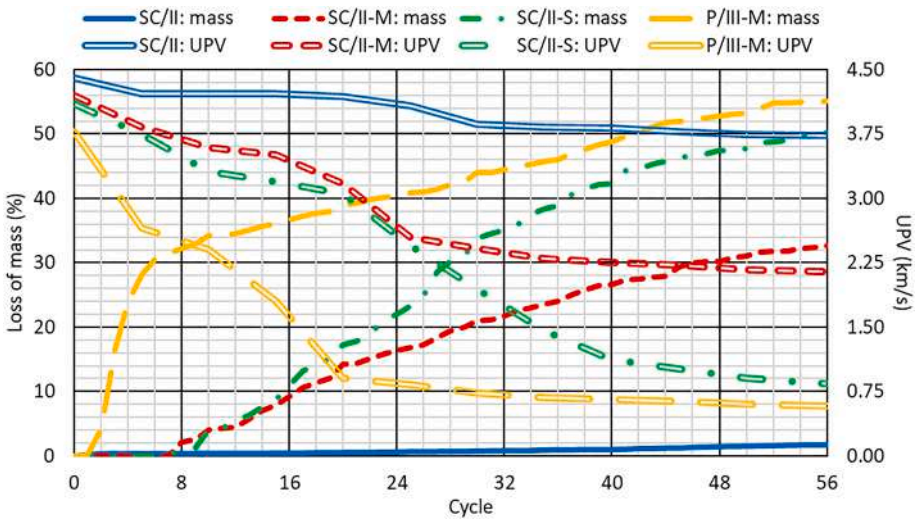

Fig. 7. Evolution of the loss of mass and UPV over the freeze/thaw test.

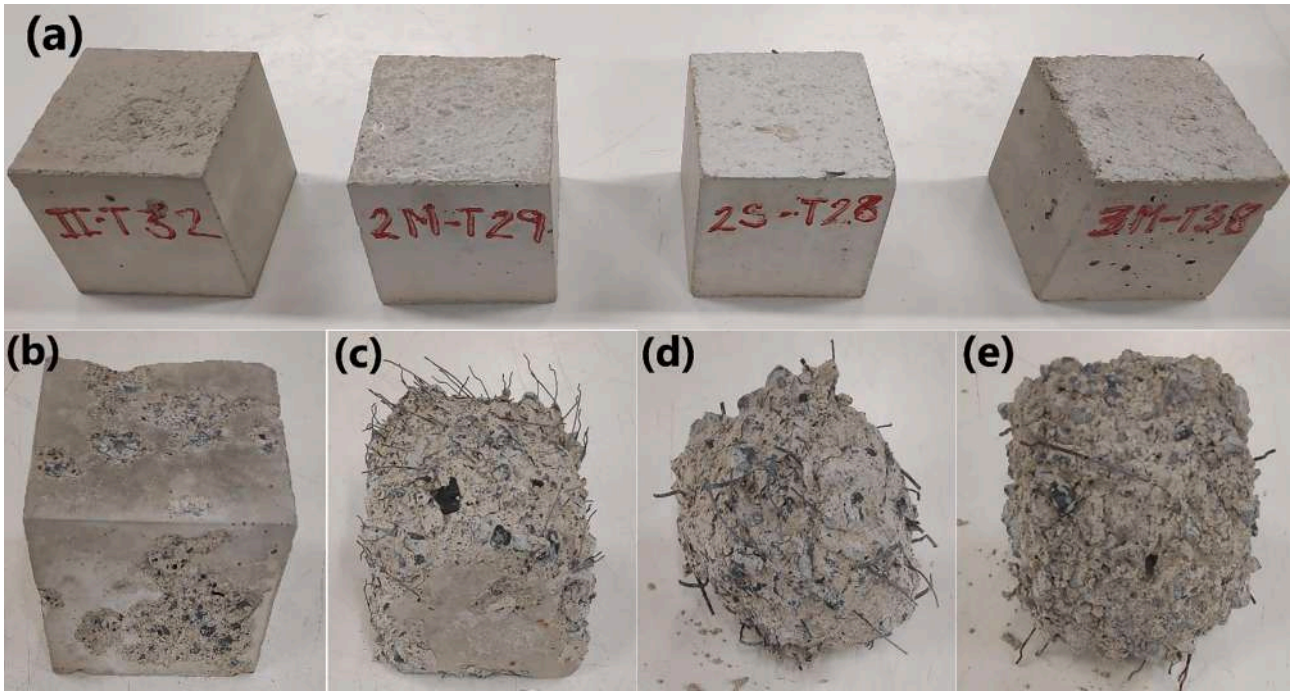

Fig. 8. (a) Specimens before the freeze/thaw tests (mixes SC/II, SC/II-M, SC/II-S and P/III-M, in that order). Specimens after the freeze/thaw test: (b) mix SC/II; (c) mix SC/II-M; (d) mix SC/II-S; (e) mix P/III-M.

results available in the literature [44], it can be affirmed that the loss of mass was higher than in concretes made with natural aggregate, due to the high micro-porosity of EAFS. The use of this alternative aggregate facilitated the penetration of NaCl solution that subsequently froze, increased in volume and cracked the aggregate [44]. The results of mass loss were consistent with the values of porosity obtained by MIP, so the higher the proportion of lower-size pores, the greater the loss of mass. However, the increase in porosity when using fibers (Table 7) hardly appeared to explain such a large increase in mass loss (Table 9), which may be due to two reasons. On the one hand, increased porosity in the outer zone (skin) of the concrete when fibers were added (Fig. 8a) favored mass loss from the outset [43]. On the other hand, the fibers interrupted the continuity of the cementitious matrix, not sewing it effectively when faced with freeze/thaw conditions [56]. Hence, the synthetic fibers were more detrimental.

- Mix P/III-M showed the highest loss of mass (55.13%), which can be explained by three aspects. First, it was the mix with the highest porosity and smallest pore sizes, so the effect of freezing water had more of a negative effect than on the other mixes. Second, it developed a weaker cementitious matrix against freeze/thaw than the SC mixes, due to its high GGBFS content [28]. Finally, it incorporated a higher EAFS content, detrimental due to the high micro-porosity of this aggregate [55]. These aspects not only increased the loss of mass, but also caused it to occur more quickly. As shown in Fig. 7, the mass loss in the 6th cycle was already 30% (null for the SC mixes), so the specimens of this concrete mix could be considered already destroyed in this cycle. In this way, their physical appearance in the 6th cycle and at the end of the test hardly differed, as shown in

Fig. 8e. The use of metallic rather than synthetic fibers was an efficient way of sewing the cementitious matrix, according to the behavior of the SC mixes. The use of metallic fibers in this mix might therefore partially compensate the described negative effects. Thus, the loss of mass of mix P/III-M was, in absolute terms, only 5% higher when compared with mix SC/II-S, manufactured with synthetic fibers.

- The evolution of the UPV during the test was in line with the aspects discussed above regarding the loss of mass, since this magnitude decreased continuously throughout the cycles. The UPV in the fiber-reinforced mixes reached values typical of completely destroyed concrete (decrease of 79.43% and 84.62% in the SC/II-S and P/III-M mixes) at the end of the test [51]. This UPV decrease was related not only to the internal damage experienced by the concrete, but also to the damage of the surface area, which allowed a poorer support of the transducers [57]. Although mix SC/II apparently experienced no mass loss during the test, remaining practically intact (Fig. 8b), its UPV did decrease by 15.30%, which was not caused by the external damage to the specimen. Since UPV is an indirect measurement of concrete quality [57], this decrease showed the existence of internal damage (micro-cracking) to the concrete that was not visible to the naked eye [58].

After completion of the cycles, the specimens were oven-dried for 72 h, and the hardened density, using the hydrostatic balance, and the compressive strength were subsequently measured. The specimens experienced practically no decrease in density (between 1% and 3%), which shows that the decrease in mass and volume during the test was in accordance with the density of the concrete. The compressive strength could only be determined on the specimens of mix SC/II after adequate conditioning (polishing), since the specimens of the other mixes were completely destroyed during the test (Fig. 8). The compressive strength value obtained, 40.94% lower than the reference value (Table 8), showed that mix SC/II did indeed experience internal damage although it never resulted in a mass loss. The micro-porosity of EAFS and the cracking it may have experienced, due to an increase in volume of the NaCl solution, might explain this phenomenon [59].

6.2. Moist/dry test

The moist/dry test is a common durability test for building façade elements made with mortar or gypsum. These elements are subjected to cyclic processes of wetting and subsequent drying, due to rain and the heat of the sun to which they are exposed [60]. Therefore, the simulation of this situation under laboratory conditions means that their behavior (expansion, contraction and variation of humidity conditions) may be observed under these environmental conditions. Concrete is also subjected to this type of phenomena when used in structures or elements exposed to the external environment [44]. Despite its more robust appearance, different studies show that its mechanical behavior can also be negatively affected by these environmental processes of wetting and drying [43].

A moist/dry test was performed on the concretes of this study, using an adaptation of the test described in the ASTM D 559 [48] standard. For that purpose, three 100x100x100-mm cubic specimens of each concrete mix were subjected to 30 moist/dry cycles. Each cycle lasted 24 h and consisted of specimen immersion in drinking water at room temperature (around 20 ± 2 °C) for 16 h and subsequent drying in an oven (temperature 70 ± 2 °C) for 8 h. The water-immersion phase simulated wetting due to rain, while the oven phase simulated drying by the heat of the sun. Both phases involved extreme environmental conditions of rain and heating that caused internal micro-cracking that damaged the concrete, which was caused by cyclic dimensional variations (expansion and contraction) and the different thermal deformability of the concrete components (aggregate, cementitious matrix and fibers). In addition, the cyclic evaporation of water absorbed by the concrete might also originate stress that caused micro-cracking [44].

In this study, at the end of each cycle, the specimens were weighed, to control the volume of water stored inside the specimens after each cycle [61]. In addition, the UPV was measured every 5 cycles to evaluate any internal damage to the concrete. The evolution of the increase in mass and UPV throughout the test is shown in Fig. 9, while Table 10 collects the total mass increase and UPV decrease after the test. At the end of the test, the specimens were dried in an oven for 72 h and their density and compressive strength were determined, the results of which are also shown in Table 10.

The increase of mass after the first two cycles (Fig. 9), with no internal damage to the concrete, was in accordance with the porosity and pore-size distribution values (Table 7). Thus, the water stored inside the specimens of mix P/III-M (more porous mix and with smaller pore sizes) meant a mass increase of 1.7%, while in mix SC/II the increase of mass was only 0.65%. The mass increase was steadily increasing (approximately linear slope) throughout the whole test for all mixes. The micro-cracking of the concrete due to cyclic wetting and drying meant that a larger volume inside the specimens could be occupied by water, with more of it being stored after the drying phase [61]. In absolute terms, the mass increase was approximately 0.5% for the SC mixes and only 0.3% for mix P/III-M from the second cycle up to the end of the test. The lower increase of mix P/III-M might perhaps be caused by lower levels of micro-cracking.

The UPV results are also shown in Fig. 9. The UPV decreased more or less steadily throughout the tests in all mixes, due to the propagation of micro-cracking into concrete. This micro-cracking was favored, as in the freeze/thaw test, by the use of EAFS, which has a higher porosity than natural aggregate [25]. However, the negative effect of using EAFS was partly compensated, due to its good mechanical behavior [43]. The final decrease of UPV is shown in the first row of Table 10. Two aspects can be observed:

- Mix P/III-M underwent the smallest decrease of this magnitude (8.88%), confirming that this was the mix with the least micro-cracking. The higher flexibility of its cementitious matrix, provided by its high GGBFS content, could be the reason why its cyclic expansion/contraction never caused severe damage [53].
- The SC mixes experienced a more notable decrease in the UPV (11.45% for mix SC/II, 19.49% for mix SC/II-M and 23.42% for mix SC/II-S). The higher stiffness of their cementitious matrix may explain this situation [28]. On the other hand, the addition of fibers implied an increase in the internal damage, possibly due to the increased porosity and smaller pore sizes associated with their use. Furthermore, the application of significant thermal oscillations may have caused the fibers, especially the synthetic ones, to experience a greater length variation than the cementitious matrix, which could cause micro-cracking [58].

The values of hardened density and compressive strength after the test (Table 10) endorsed the behavior observed through the UPV measurements. All the mixes experienced a decrease in density, due to the increase in volume caused by micro-cracking without mass variation. The compressive strength also decreased after the test, due to the internal damage within the concrete. So, mix P/III-M underwent a loss of both density and compressive strength of 0.8% and 13.8%, respectively, less than the losses of mix SC/II-S, of 3.1% and 40.3%, respectively. It is important to indicate that all the damage caused by this test was microstructural, since the specimens were never damaged at the macroscopic level. This point is shown in Fig. 10 for a representative specimen of mix P/III-M, in which no significant differences were observed in the results before and after the moist/dry test.

6.3. Sulfate-attack test

Sulfate attack on structural concrete is common in marine

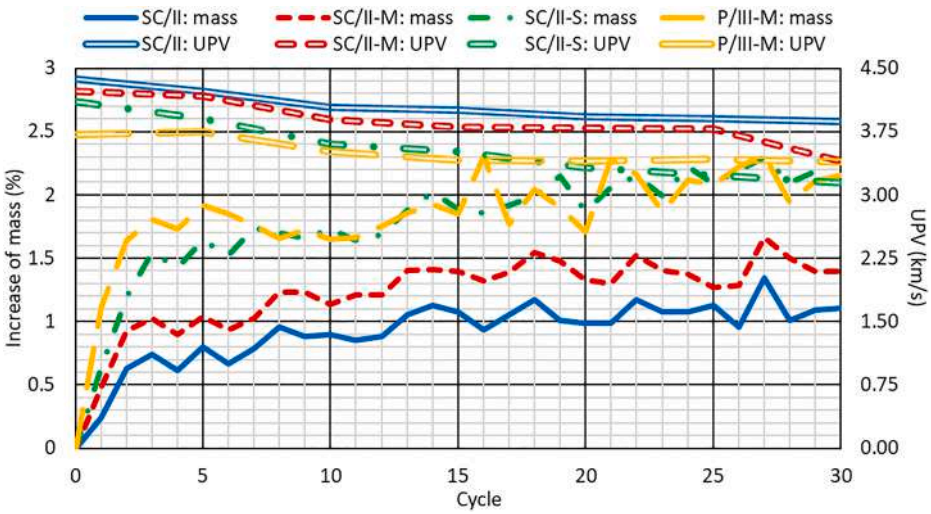

Fig. 9. Evolution of the increase of mass and UPV throughout the moist/dry test.

Table 10
Results of the moist/dry test (standard deviation in brackets).

Mix	SC/II	SC/II-M	SC/II-S	P/III-M
Total increase of mass (%)	1.10 (0.12)	1.40 (0.13)	2.09 (0.17)	2.15 (0.15)
Total UPV decrease (%)	11.45 (0.89)	19.49 (1.23)	23.42 (1.27)	8.88 (1.02)
Hardened density after the test (Mg/m^3)	2.62 (0.01)	2.52 (0.03)	2.46 (0.02)	2.63 (0.02)
Average loss of hardened density (%)	0.4 (0.01)	1.9 (0.01)	3.1 (0.02)	0.8 (0.01)
Compressive strength after the test (MPa)	65.0 (3.0)	51.4 (2.3)	41.2 (1.9)	40.7 (1.3)
Average loss of compressive strength (%)	26.39 (3.41)	30.82 (2.21)	40.29 (4.24)	13.77 (1.88)

environments [27]. Sulfates can corrode the reinforcements, cause dimensional variations due to the increase of volume as the water evaporates, and even micro-crack the concrete, worsening its mechanical behavior. Going a step further, sulfates can react with the products from cement hydration, amplifying these negative effects [49]. However, cements with GGBFS are sulfate-resistant (EN 197 [35]), *i.e.*, they are not affected by sulfates. In this way, these cements have traditionally been used for the stabilization of sulfate-rich-subterranean-water or gypsum-rich soils [33].

The sulfate-attack test was performed according to ASTM C 1012 [48]. Three 100x100x100-mm cubic specimens were subjected to 15 cycles of 24 h comprising three stages. The first stage consisted of the immersion of the specimens in an aqueous solution with 14% by mass of $Na_2SO_4{\cdot}10H_2O$ for 5 h. Subsequently, in the second stage, the specimens were oven-dried for 17 h at 110 ± 2 °C. The cycle ended with cooling at room temperature (20 ± 2 °C) for 2 h. After each cycle, the specimens were weighed to evaluate the increase in mass due to the water and solidified sulfate salt stored inside. In addition, the UPV was measured every 5 cycles to evaluate any internal damage (micro-cracking) to the concrete. The evolution of these magnitudes throughout the test is depicted in Fig. 11, which shows that:

- The initial increase of mass was in line with the porosity of the mixes (Table 7). Thus, mix P/III-M was the one with the highest proportion of pores smaller than 100 nm, so it exhibited the highest mass increase (0.80%). Moreover, the mass increase remained practically unchanged with respect to the initial value throughout the test.
- The initial UPV values were lower than those measured in the freeze/thaw and moist/dry tests because the solidified salts inside concrete reduced it [44]. On the other hand, the decrease in UPV over the 15 cycles was minimal (7.42% for mix P/III-M, and 9–12% for the SC mixes, Table 11). Therefore, the micro-cracking they experienced was reduced, which explains the null variation in mass increase. It seems that increasing the EAFS content had no negative effect [43],

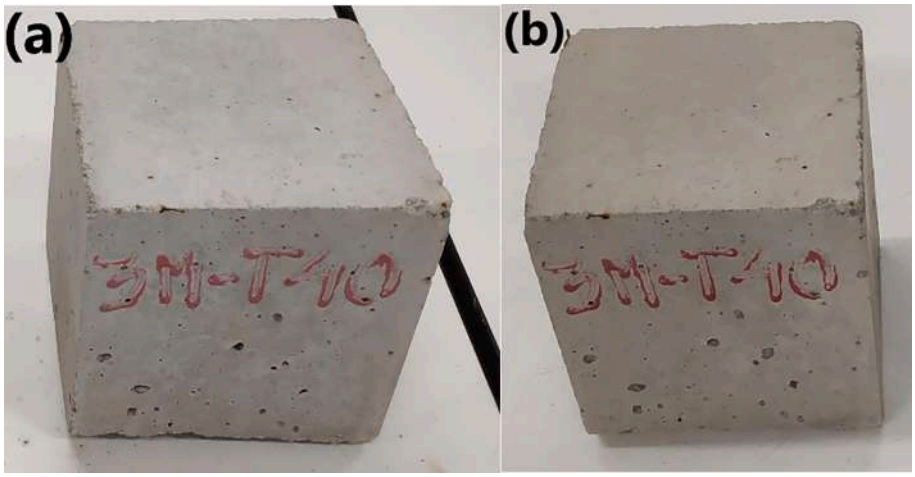

Fig. 10. Specimen of mix P/III-M before (a) and after (b) the moist/dry test.

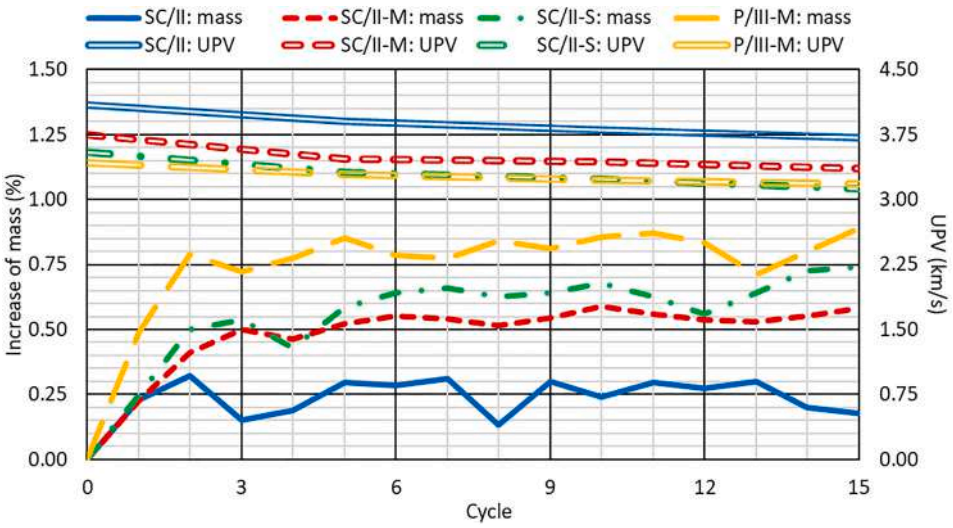

Fig. 11. Evolution of the increase of mass and UPV throughout the sulfate-attack test.

probably due to the salt clogging up its pores, which prevented cracking propagation. The fibers had a negative effect, as they increased porosity and their length increased at high temperatures. The increased GGBFS content in the cementitious matrix produced a more flexible concrete, which reduced the damage [28].

After the test, the specimens showed no apparent damage. As shown in Fig. 12 for a specimen of the mix P/III-M, only a certain yellowish color and oxidation of the metallic fibers were observed. In addition, other aspects listed in Table 11 were analyzed:

- The dimensional variation was always less than 0.10%, the limit established by ASTM C 1012 [48] for dimensionally-stable concretes.
- The density of all the mixes was increased. Thus, the small dimensional increment was lower than the mass increase due to salt crystallization [61]. Mix SC/II-S experienced the largest increase, 2.0%, due to its greater micro-cracking and, therefore, greater space to be occupied by solidified salt.
- The decreases in compressive strength were less than those in the moist/dry test, due to less micro-cracking. Again, mix P/III-M had the lowest loss of strength (7.42%), due to its more elastic cementitious matrix and the fact that fiber oxidation was not very negative, while mix SC/II-S showed the highest decrease, 22.75%. These values were consistent with the UPV variations.

Table 11
Results of the sulfate-attack test (standard deviation in brackets).

Mix	SC/II	SC/II-M	SC/II-S	P/III-M
Total increase of mass (%)	0.18 (0.03)	0.58 (0.07)	0.74 (0.09)	0.89 (0.10)
Total UPV decrease (%)	9.29 (0.97)	10.40 (1.23)	11.83 (1.17)	7.29 (0.76)
Dimensional variation (%)	+0.04 (0.00)	+0.06 (0.01)	+0.09 (0.01)	+0.04 (0.00)
Hardened density after the test (Mg/m^3)	2.67 (0.03)	2.60 (0.02)	2.59 (0.03)	2.68 (0.02)
Average increase of hardened density (%)	1.5 (0.06)	1.2 (0.04)	2.0 (0.03)	1.1 (0.03)
Compressive strength after the test (MPa)	74.9 (3.4)	56.4 (3.5)	53.3 (2.9)	43.7 (1.5)
Average loss of compressive strength (%)	15.18 (1.89)	17.73 (2.31)	22.75 (1.95)	7.42 (1.43)

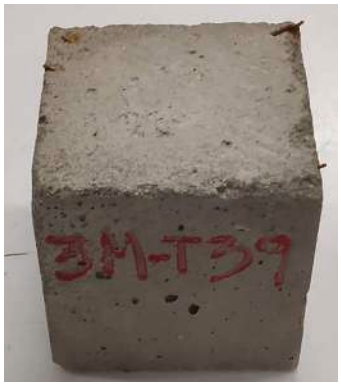

Fig. 12. Appearance of a specimen from mix P/III-M after the sulfate-attack test (initial appearance shown in Fig. 10a).

6.4. Chloride-penetration test

The penetration of chlorides into concrete can lead to corrosion of reinforcements, with the ensuing risk of structural failure [27]. The main risk occurs in concrete elements submerged in salt water, although in a marine environment the presence of this type of compound in the air can also be dangerous [62].

In this study, the chloride-penetration test was performed according to EN 12390-11 [35]. Two 100x200-mm cylindrical specimens per mix were cut in half, obtaining four 100x100-mm cylindrical specimens. Subsequently, a test similar to the capillary-water-absorption test was performed on them to simulate a natural process of chloride penetration into concrete. To do so, the four specimens were waterproofed on their curve face and their cut face was placed in contact with a 2 ± 1-mm-thick layer of an aqueous solution containing 3.5% NaCl by mass (NaCl concentration in seawater). The aqueous solution was absorbed by concrete through capillary action, the chlorides being retained inside it. Two test periods were chosen, 28 days (4 weeks) and 126 days (18 weeks), in which the specimens were in contact with the salt solution (two 100x100-mm cylindrical specimens tested for each period). The feasibility of using the concretes designed in the presence of chlorides could have simply been analyzed over a 28-day period [63]. However, a longer period of time was also selected to analyze the evolution of chloride penetration over time.

The specimens were weighed at the beginning and at the end of each test period, thus determining the porosity of the concrete occupied by

the saline solution from the density of seawater (1.0267 Mg/m^3), as shown in Table 12. In addition, the average depth of chloride penetration was determined using the colorimetric method [64]. To do so, the specimens were split in half (Brazilian test) and sprayed with an $AgNO_3$ solution. The area with presence of chlorides turned white, showing a U-shape (Fig. 13), as the reaction of Cl^- ions with $AgNO_3$ produced AgCl that appeared whitish in color [64]. This test method was chosen for its simplicity and the low carbonation of the mixes, since they were cured in the laboratory under ambient conditions. Furthermore, the real existence of chlorides in the whitish zone was controlled in spot specimens by chemical analysis (EN 12390-11 [35]). The evolution of the chloride penetration over time is depicted in Fig. 14.

As expected, the porosity occupied by the saline solution (Table 12) agreed with the MIP porosity of the mixes (Table 7), in the sense that the higher the MIP porosity, the higher its occupation by the saline solution. However, there was no exact proportionality between them, which is explained by the interconnection between the pores and their size [33]. Mix SC/II, with a MIP porosity of 9.5%, showed a greater number of isolated pores, which were also smaller in size and which hindered the entry of the solution (occupied porosity of 4.59% at 126 days). However, the other mixtures showed greater interconnection between their pores, possibly due to the presence of fibers or large amounts of GGBFS [38,43]. Thus, mix P/III-M, with an MIP porosity of 14.7%, presented an occupied porosity of 10.0% at 126 days.

The chloride-penetration results (Table 12) followed the same trend. Therefore, a higher occupied porosity led to higher levels of chloride penetration. According to the results available in the bibliography [27,62], the chloride depths were around 25% higher than those obtained in SCC with natural aggregate, because the addition of EAFS increased the porosity of the cementitious matrix, due to the high micro-porosity of this by-product. Furthermore, the chloride footprint depth at 28 days was in all cases 60–65% of the footprint at 126 days. Thus, chloride penetration over time (Fig. 14) evolved according to the square root of time, as reported in the literature [65] and regulations [66]. A double square root model was the best fit in all cases, with coefficients R^2 of 95–99%.

Chloride penetration in 28 days, comparable with the degradation of a concrete exposed to a marine environment throughout its service life [63], was always lower than the standard concrete cover of the reinforcements for this type of environment (35–40 mm) [66]. The use of these mixtures in those environments would be adequate, although mix P/III-M should be used with caution, as the average depth of the footprint, around 33 mm, was close to the limits of the regulations [66].

6.5. Carbonation test

Carbonation of concrete can cause the corrosion of the reinforcements, in the same way as chlorides [65]. It is a process that naturally occurs at a very slow rate, in which $Ca(OH)_2$ from hydrated cement reacts with atmospheric CO_2 to produce $CaCO_3$ [43]. In this case,

Table 12
Results of the chloride-penetration test (standard deviation in brackets).

Time (days)	Mix	SC/II	SC/II-M	SC/II-S	P/III-M
28	Weight increase (g)	22.6 (1.2)	38.0 (2.6)	49.5 (2.9)	60.6 (4.2)
	Occupied porosity (%)	2.80 (0.24)	4.71 (0.27)	6.14 (0.41)	7.52 (0.48)
	Average footprint depth (mm)	14.48 (0.34)	25.71 (0.58)	27.79 (0.64)	33.31 (0.71)
126	Weight increase (g)	37.0 (1.9)	61.2 (4.1)	71.1 (4.8)	80.6 (3.9)
	Occupied porosity (%)	4.59 (0.22)	7.59 (0.36)	8.82 (0.43)	10.0 (0.44)
	Average footprint depth (mm)	23.18 (0.41)	42.14 (0.97)	45.30 (0.87)	55.84 1.03)

Fig. 13. Chloride footprint in 28 days in a specimen of mix SC/II.

an accelerated-carbonation test was performed as per EN 13295 [35]. For that purpose, four 100x100x100-mm cubic specimens of each mix were placed in a carbonation chamber for 28 and 126 days, the same time periods as in the chloride-penetration test. Two specimens were tested for each exposure period. This chamber presented an atmosphere with a CO_2 concentration between 10% and 20%, a relative humidity between 50% and 60%, and a temperature of 20 ± 2 °C.

Before the test, the dimensions and the UPV of the specimens were measured, the latter magnitude presenting values similar to those initially obtained in the freeze/thaw and moist/dry tests. At the end of each exposure period, the specimens were weighed, their hardened density was determined, and their UPV and dimensional variation were evaluated. The results are presented in Table 13. Finally, the specimens were split in half and sprayed with an aqueous phenolphthalein solution as specified in UNE 112011 [67], which turned reddish-purple for pH values above 9.5, pink for pH values between 8 and 9.5, and remained colorless for pH values below 8. The colorless zones were the carbonated zones (Fig. 15), in which the average depth of carbonation was determined (Table 13 and Fig. 16).

The results showed a very similar trend to those of the chloride-penetration test. Thus, mix SC/II showed the best results, mixes SC/II-M and SC/II-S presented intermediate results, very similar to each other, and mix P/III-M behaved worst of all. These results demonstrate the strong dependence between concrete carbonation and porosity (Table 7) [22].

All the mixes experienced a minimal increase in weight, and practically no dimensional variation, which led to a small increase in density. The formation of carbonates, with a higher molecular weight than calcium hydroxide, explain this phenomenon [65]. The minimum increase occurred in mix SC/II (0.38% in 126 days), while mix P/III-M experienced a density increase of 0.64% at 126 days. The increased porosity and interconnection between pores led to increased carbonation and carbonate formation [43]. In addition, the presence of large amounts of GGBFS could also favor this carbonation process, as reported in the literature [22]. The variation of UPV showed no clear trend, since in some cases this magnitude increased after the carbonation period and in others it decreased. It can therefore be stated that, as expected, the carbonation process caused no internal damage to the concrete as UPV only exhibited the typical oscillations of an experimental measurement.

The carbonation depth showed the same trend, in so far as the greater the depth, the higher the porosity level and the proportion of nano-sized pores. Again, the micro-porosity of EAFS was negative compared to the use of natural aggregate [44]. Furthermore, the increased porosity of concrete when adding fibers and adjusting the water content to maintain flowability offset the beneficial effect of fibers

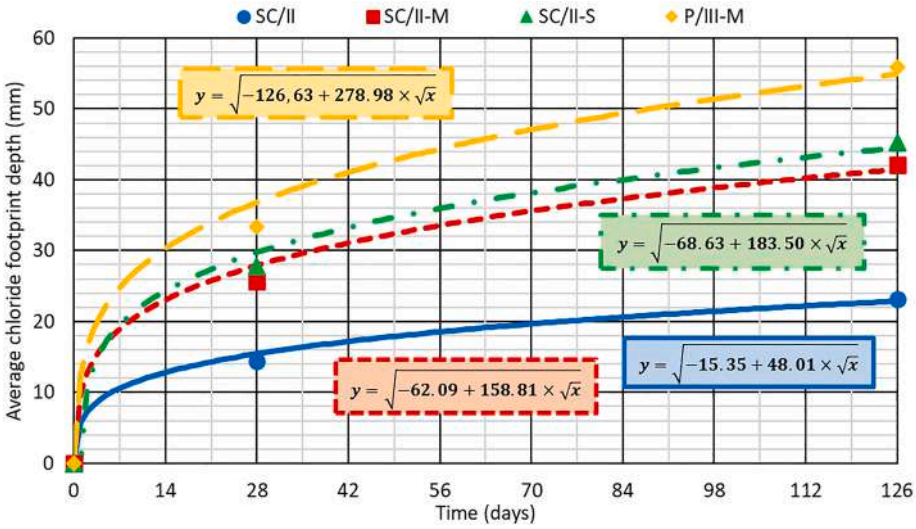

Fig. 14. Evolution of average chloride footprint depth over time.

Table 13
Results of the carbonation test (standard deviation in brackets).

Time (days)	Mix	SC/II	SC/II-M	SC/II-S	P/III-M
28	Weight increase (%)	0.07 (0.01)	0.09 (0.01)	0.10 (0.01)	0.32 (0.02)
	Dimensional variation (%)	+0.00 (0.00)	+0.00 (0.00)	+0.00 (0.00)	+0.01 (0.00)
	Hardened density after the test (Mg/m^3)	2.63 (0.02)	2.58 (0.02)	2.55 (0.01)	2.66 (0.02)
	Hardened density increase (%)	0.24 (0.01)	0.29 (0.01)	0.31 (0.01)	0.49 (0.01)
	UPV variation (%)	−1.26 (0.13)	+0.51 (0.11)	−1.29 (0.15)	+0.97 (0.14)
	Average carbonation depth (mm)	7.1 (0.34)	9.8 (0.43)	12.0 (0.49)	16.8 (0.64)
126	Weight increase (g)	0.12 (0.01)	0.14 (0.01)	0.17 (0.01)	0.46 (0.02)
	Dimensional variation (%)	+0.00 (0.00)	+0.00 (0.00)	+0.01 (0.00)	+0.02 (0.00)
	Hardened density (Mg/m^3)	2.64 (0.02)	2.58 (0.01)	2.55 (0.01)	2.67 (0.03)
	Hardened density increase (%)	0.38 (0.02)	0.39 (0.02)	0.41 (0.01)	0.64 (0.02)
	UPV variation (%)	−0.54 (0.14)	−1.01 (0.23)	−0.89 (0.09)	+1.12 (0.13)
	Average carbonation depth (mm)	12.7 (0.56)	17.1 (0.57)	19.2 (0.41)	25.4 (1.13)

in the carbonation of EAFS concrete observed in other studies [43]. The effect of synthetic fibers was more detrimental, so that mix SC/II-S had a carbonation depth at 126 days of 19.2 mm compared to 17.1 mm of mix SC/II-M. The use of large amounts of GGBFS further facilitated the carbonation of the concrete, obtaining a value of 25.4 mm at 126 days in mix P/III-M. Despite this, the carbonation depth at 126 days (a period that can be assimilated to the service life of any structure in terms of carbonation) was always less than 30 mm (Table 13), a common concrete cover for the reinforcements in an outdoor environment [66]. Finally, considering the evolution of the carbonation depth over time, the carbonation depth at 28 days was always 60–70% of the depth at 126 days, showing a trend with coefficients R^2 of 95–99% (Fig. 16), by the square root of time, and in relation to chloride penetration, as has been reported in the literature [65].

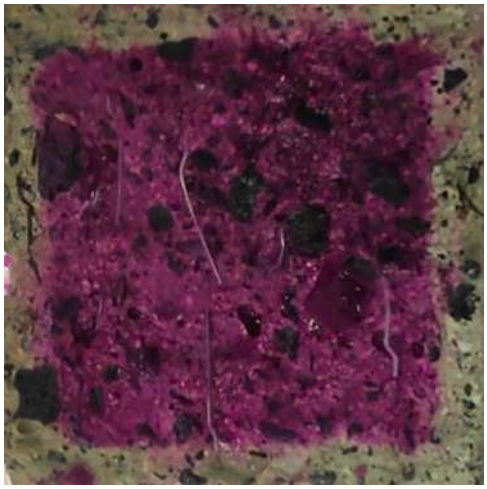

Fig. 15. Carbonated area of a representative specimen of mix SC/II-M in 126 days.

6.6. SO_2-attack test (Kesternich test)

Many industrial buildings have a foundation slab made of concrete reinforced with fibers, usually metallic, to reduce shrinkage. In addition, in certain industrial environments there are SO_2-rich atmospheres, which undoubtedly favor the corrosion of any steel element. Therefore, it is possible that the behavior of concrete in these environments may be adversely affected by the corrosion of the fibers [43]. On the other hand, the exposure of concrete to SO_2 can cause the expansion of the cementitious matrix, due to the formation of ettringite and thaumasite, which also reduces strength [68].

The procedure for performing the Kesternich test or SO_2-attack test is described in the EN ISO 6988 standard [35] and is usually applied to evaluate the corrosion of metals. In this case, the same procedure was applied to the developed concrete mixes. Thus, three 100x100x100-mm cubic specimens per mix were subjected to 15 cycles of 24 h consisting of exposure to water vapor (100% relative humidity) saturated with SO_2 at 40 ± 2 °C for 8 h followed by air-cooling at room temperature (20 ± 2 °C) for 16 h. Upon completion of the test and oven drying of the tested specimens for 72 h, weight, UPV, compressive strength and hardened density variations were evaluated. In addition, dimensional variation, a determining factor in the volumetric stability of the mixes, was

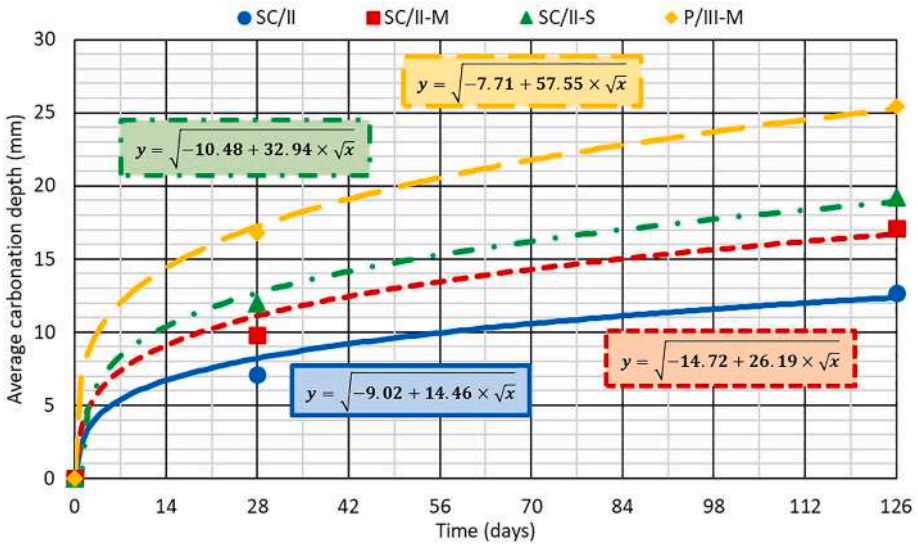

Fig. 16. Evolution of average carbonation depth over time.

evaluated by measuring the length of each side of the specimens before and after the test. All these results are shown in Table 14.

All the mixes experienced an increase in weight and volume (dimensional variation), due to the formation of ettringite and thaumasite, which in turn led to a slight increase in hardened density [68]. The results showed that the increase in density was conditioned by porosity and pore size, which facilitated the entry of SO_2 into the concrete. Thus, mix SC/II-S showed a greater increase in density than mix SC/II (0.48% vs. 0.14%). However, the presence of metallic fibers and their corrosion, which is depicted in Fig. 17, appears to have contributed to that effect, since mixes SC/II-M and P/III-M presented higher density increases. The UPV never revealed the existence of internal damage, although the compressive strength decreased in all the mixtures. Once again, a higher porosity and the presence of fibers was the most unfavorable situation, so that mixes SC/II (lowest porosity) and P/III-M (highest porosity) underwent compressive strength decreases of 5.6% and 12.7%, respectively. These decreases in strength were in line with the results reported in the available bibliography [43]. Nevertheless, there is no real problem, provided that an adequate safety coefficient for compressive strength is considered in the structural design [66].

7. Conclusions

This study has evaluated the performance under field conditions of a fiber-reinforced Self-Compacting Concrete (SCC) made with 100% coarse and fine Electric Arc Furnace Slag (EAFS) as aggregate and Ground Granulated Blast Furnace Slag (GGBFS) as binder. Tests were performed to simulate the strength and stiffness development by concrete in real-structure conditions (core drilling). Furthermore, durability tests that simulated numerous environmental conditions (freeze/thaw, moist/dry, sulfate attack, chloride penetration, carbonation, and SO_2 attack) were also conducted. From the aspects discussed throughout the article, the following conclusions can be drawn:

- The addition of fibers, both metallic and synthetic, implied an increase in the water content to preserve flowability, which in turn resulted in an increase in porosity and a decrease in strength and stiffness. The addition of large amounts of GGBFS had the same effect, besides preventing the achievement of self-compactability, due to the high specific gravity of EAFS and the reduced dragging capacity of this binder.
- The long-term compressive strength and stiffness of the concretes developed when used in a real ambient-cured structure were similar to those obtained in specimens cured for 90 days in a moist chamber.
- The use of fibers in an EAFS SCC had no beneficial effect under freeze/thaw phenomena, due to the increased porosity of the cementitious matrix. Thus, they promoted quicker deterioration of concrete. The combination of 70% GGBFS with metallic fibers resulted in a dramatic deterioration of the specimen, whose loss of mass after six cycles was critical.

Fig. 17. Detail of the corrosion of external metallic fibers after the SO_2-attack test on a mix SC/II-M specimen.

Table 14
Results of the SO_2-attack test (standard deviation in brackets).

Mix	SC/II	SC/II-M	SC/II-S	P/III-M
Weight increase (%)	0.78	1.47	1.03	1.84
Dimensional variation (%)	+0.01	+0.03	+0.01	+0.04
Hardened density after the test (Mg/m^3)	2.63	2.58	2.55	2.66
Hardened density increase (%)	0.14	0.77	0.48	0.62
UPV variation (%)	+0.85	+1.23	−1.44	−0.27
Compressive strength after the test (MPa)	83.4	65.6	62.9	41.2
Loss of compressive strength (%)	5.55	11.71	8.84	12.71

- The increase of the water content when adding fibers, to achieve adequate fresh behavior, led to increased porosity in the mixes. This aspect, as well as the length increase of the fibers at high temperatures, favored internal micro-cracking of the SCC against cyclic moist/dry and sulfate-attack processes. On the other hand, the addition of GGBFS created a more flexible cementitious matrix that better withstood thermal expansion/contraction, varying moisture conditions and sulfate salt expansion.
- Chloride penetration and carbonation depth depended on the porosity of the mixtures, so they were both increased following the addition of fibers and GGBFS. Both magnitudes evolved with the square root of time, presenting values adequate to the concrete cover of the reinforcements for exposure times that simulated the service life of a structure.
- SO_2 attack caused a decrease in strength, due to the expansion of the cementitious matrix. Corrosion of the metallic fibers slightly amplified this phenomenon.

In general, it can be concluded that, despite the high micro-porosity of the EAFS, the durability behavior of the concretes was correct, fulfilling the requirements established in the regulations. Therefore, the mixtures produced, with the simultaneous use of EAFS, GGBFS and fibers, would be suitable for structural elements exposed to low temperatures, high ambient humidity and marine environments. However, the addition of fibers and large volumes of GGBFS in an SCC with high amounts of EAFS must be carefully performed, in order to balance the fresh behavior and the increased porosity and proportion of nano-sized pores, which facilitates the penetration of harmful external agents.

CRediT authorship contribution statement

Vanesa Ortega-López: Conceptualization, Supervision, Formal analysis, Data curation, Writing – original draft, Project administration, Funding acquisition. **Flora Faleschini:** Methodology, Data curation, Supervision, Writing – review & editing, Project administration. **Carlo Pellegrino:** Methodology, Formal analysis, Supervision, Writing – review & editing, Project administration. **Víctor Revilla-Cuesta:** Conceptualization, Methodology, Formal analysis, Data curation, Writing – original draft, Writing – review & editing. **Juan M. Manso:** Conceptualization, Formal analysis, Writing – review & editing, Project administration, Funding acquisition.

Declaration of Competing Interest

The authors declare that they have no known competing financial interests or personal relationships that could have appeared to influence the work reported in this paper.

Acknowledgements

The authors wish to express their gratitude to: Spanish Ministry of Universities within the framework of the State Program for the Promotion of Talent and its Employability in R + D + i, State Mobility Subprogram, of the State Plan for Scientific and Technical Research and Innovation 2017-2020 [PRX21/00007]; the Spanish Ministry of Universities, MICINN, AEI, EU and ERDF [grant numbers PID2020-113837RB-I00; 10.13039/501100011033; FPU17/03374]; the Junta de Castilla y León (Regional Government) and ERDF [grant numbers UIC-231; BU119P17]; Youth Employment Initiative (JCyL) and ESF [grant number UBU05B_1274]; and finally, to the University of Burgos [grant numbers SUCONS, Y135.GI] and the University of Padova.

References

[1] H. Okamura, M. Ouchi, Self-compacting concrete, J. Adv. Concr. Technol. 1 (2003) 5–15. 10.3151/jact.1.5.
[2] M. Ouchi, Y. Edamatsu, K. Ozawa, H. Okamura, Simple evaluation method for interaction between coarse aggregate and mortar's particles in self-compacting concrete, Trans. Jpn. Concr. Inst. 21 (1999) 1–6.
[3] A. Santamaría, J.J. González, M.M. Losáñez, M. Skaf, V. Ortega-López, The design of self-compacting structural mortar containing steelmaking slags as aggregate, Cem. Concr. Compos. 111 (2020), 103627, https://doi.org/10.1016/j.cemconcomp.2020.103627.
[4] B.I.O. Koura, M. Hosseinpoor, A. Yahia, Coupled effect of fine mortar and granular skeleton characteristics on dynamic stability of self-consolidating concrete as a diphasic material, Constr. Build. Mater. 263 (2020), 120131, https://doi.org/10.1016/j.conbuildmat.2020.120131.
[5] A. Santamaría, A. Orbe, M.M. Losañez, M. Skaf, V. Ortega-Lopez, J.J. González, Self-compacting concrete incorporating electric arc-furnace steelmaking slag as aggregate, Mater. Des. 115 (2017) 179–193, https://doi.org/10.1016/j.matdes.2016.11.048.
[6] S. Santos, P.R. da Silva, J. de Brito, Self-compacting concrete with recycled aggregates – a literature review, J. Build. Eng. 22 (2019) 349–371, https://doi.org/10.1016/j.jobe.2019.01.001.
[7] M. Ouchi, M. Hibino, H. Okamura, Effect of superplasticizer on self-compactability of fresh concrete, Transp. Res. Rec. 1574 (1) (1997) 37–40, https://doi.org/10.3141/1574-05.
[8] M. Ouchi, M. Hibino, T. Sugamata, H. Okamura, Quantitative evaluation method for the effect of superplasticizer in self-compacting concrete, Trans. Jpn. Concr. Inst. 22 (2000) 15–20.
[9] EFNARC, Specification Guidelines for Self-compacting Concrete, European Federation of National Associations Representing producers and applicators of specialist building products for Concrete (2002).
[10] V. Arularasi, P. Thamilselvi, S. Avudaiappan, E.I. Saavedra Flores, Energy consumption of self-compacting concrete during mixing and its impact on the yield stress measured in the ready-mix concrete plant, Adv. Civ. Eng. (2021) 6664577, https://doi.org/10.1155/2021/6664577.
[11] J. Xie, S.C. Kou, H. Ma, W.-J. Long, Y. Wang, T.-H. Ye, Advances on properties of fiber reinforced recycled aggregate concrete: experiments and models, Constr. Build. Mater. 277 (2021) 122345, https://doi.org/10.1016/j.conbuildmat.2021.122345.
[12] L. Zhou, S. Guo, Z. Zhang, C. Shi, Z. Jin, D. Zhu, Mechanical behavior and durability of coral aggregate concrete and bonding performance with fiber-reinforced polymer (FRP) bars: a critical review, J. Clean. Prod. 289 (2021) 125652, https://doi.org/10.1016/j.jclepro.2020.125652.
[13] S. Cabrera, A. González, R. Rotondaro, Compressive Strength in Compressed Earth Blocks. Comparison Between Different Test Methods, Inf. Constr. 72 (560) (2020) 1-12. 10.3989/ic.70462.
[14] V. Ortega-López, A. García-Llona, V. Revilla-Cuesta, A. Santamaría, J.T. San-José, Fiber-reinforcement and its effects on the mechanical properties of high-workability concretes manufactured with slag as aggregate and binder, J. Build. Eng. 43 (2021), 102548, https://doi.org/10.1016/j.jobe.2021.102548.
[15] R. Lanti, M. Martínez, Biaxial bending and axial load in reinforced concrete sections. Numerical approach, Inf. Constr. 72 (558) (2020) 1–9. 10.3989/ic.69148.
[16] J.A. Fuente-Alonso, V. Ortega-López, M. Skaf, Á. Aragón, J.T. San-José, Performance of fiber-reinforced EAF slag concrete for use in pavements, Constr. Build. Mater. 149 (2017) 629–638, https://doi.org/10.1016/j.conbuildmat.2017.05.174.
[17] M.S. Ammari, M. Bederina, B. Belhadj, A. Merrah, Effect of steel fibers on the durability properties of sand concrete with barley straws, Constr. Build. Mater. 264 (2020), 120689, https://doi.org/10.1016/j.conbuildmat.2020.120689.
[18] S. Pranav, S. Aggarwal, E.-H. Yang, A. Kumar Sarkar, A. Pratap Singh, M. Lahoti, Alternative materials for wearing course of concrete pavements: a critical review, Constr. Build. Mater. 236 (2020) 117609, https://doi.org/10.1016/j.conbuildmat.2019.117609.
[19] V. Revilla-Cuesta, M. Skaf, F. Faleschini, J.M. Manso, V. Ortega-López, Self-compacting concrete manufactured with recycled concrete aggregate: an overview, J. Clean. Prod. 262 (2020) 121362, https://doi.org/10.1016/j.jclepro.2020.121362.
[20] B. Xiong, C. Demartino, J. Xu, A. Simi, G.C. Marano, Y. Xiao, High-strain rate compressive behavior of concrete made with substituted coarse aggregates: recycled crushed concrete and clay bricks, Constr. Build. Mater. 301 (2021), 123875, https://doi.org/10.1016/j.conbuildmat.2021.123875.
[21] A.R. Khan, S. Fareed, M.S. Khan, Use of recycled concrete aggregates in structural concrete, Sustain. Constr. Mater. Technol. 2 (2019).
[22] A.S. Brand, E.O. Fanijo, A review of the influence of steel furnace slag type on the properties of cementitious composites, Appl. Sci. 10 (22) (2020) 8210, https://doi.org/10.3390/app10228210.
[23] European Association representing metallurgical slag producers and processors (EUROSLAG). Available online: https://www.euroslag.com.
[24] Y. Jiang, T.C. Ling, C. Shi, S.Y. Pan, Characteristics of steel slags and their use in cement and concrete—a review, Resour. Conserv. Recycl. 136 (2018) 187–197, https://doi.org/10.1016/j.resconrec.2018.04.023.
[25] I. Arribas, J. San-José, I. Vegas, J. Hurtado, J. Chica, Application of steel slag concrete in the foundation slab and basement wall of the Tecnalia kubik building, in: Proceedings of the 6th European Slag Conference, 2010, pp. 251–264.
[26] N.H. Roslan, M. Ismail, N.H.A. Khalid, B. Muhammad, Properties of concrete containing electric arc furnace steel slag and steel sludge, J. Build. Eng. 28 (2020), 101060, https://doi.org/10.1016/j.jobe.2019.101060.
[27] I. Sosa, P. Tamayo, J.A. Sainz-Aja, C. Thomas, J. Setién, J.A. Polanco, Durability aspects in self-compacting siderurgical aggregate concrete, J. Build. Eng. 39 (2021), 102268, https://doi.org/10.1016/j.jobe.2021.102268.

[28] A.S. Albidah, Effect of partial replacement of geopolymer binder materials on the fresh and mechanical properties: a review, Ceram. Int. 47 (11) (2021) 14923–14943, https://doi.org/10.1016/j.ceramint.2021.02.127.
[29] E.R. Teixeira, A. Camões, F.G. Branco, J.C. Matos, Effect of biomass fly ash on fresh and hardened properties of high volume fly ash mortars, Crystals 11 (3) (2021) 233, https://doi.org/10.3390/cryst11030233.
[30] B. Cantero, M. Bravo, J. de Brito, I.F. Sáez del Bosque, C. Medina, Water transport and shrinkage in concrete made with ground recycled concrete-additioned cement and mixed recycled aggregate, Cem. Concr. Compos. 118 (2021), 103957, https://doi.org/10.1016/j.cemconcomp.2021.103957.
[31] V.A. Nunes, P.H.R. Borges, Recent advances in the reuse of steel slags and future perspectives as binder and aggregate for alkali-activated materials, Constr. Build. Mater. 281 (2021), 122605, https://doi.org/10.1016/j.conbuildmat.2021.122605.
[32] R. Maddalena, J.J. Roberts, A. Hamilton, Can Portland cement be replaced by low-carbon alternative materials? a study on the thermal properties and carbon emissions of innovative cements, J. Clean. Prod. 186 (2018) 933–942, https://doi.org/10.1016/j.jclepro.2018.02.138.
[33] H.L. Wu, F. Jin, Y.L. Bo, Y.J. Du, J.X. Zheng, Leaching and microstructural properties of lead contaminated kaolin stabilized by GGBS-MgO in semi-dynamic leaching tests, Constr. Build. Mater. 172 (2018) 626–634, https://doi.org/10.1016/j.conbuildmat.2018.03.164.
[34] J. Pacheco, R.B. Polder, Critical chloride concentrations in reinforced concrete specimens with ordinary Portland and blast furnace slag cement, Heron 61 (2) (2016) 99–119.
[35] EN-Euronorm, Rue de stassart, 36. Belgium-1050 Brussels, European Committee for Standardization.
[36] R. Mohana, S. Prabavathy, S.M. Leela Bharathi, Sustainable utilization of industrial wastes for the cleaner production of ferrocement structures: a comprehensive review, J. Clean. Prod. 291 (2021) 125916, https://doi.org/10.1016/j.jclepro.2021.125916.
[37] S. Dey, V.V.P. Kumar, K.R. Goud, S.K.J. Basha, State of art review on self compacting concrete using mineral admixtures, J. Build. Pathol. Rehabilit. 6 (1) (2021) 18, https://doi.org/10.1007/s41024-021-00110-9.
[38] V. Revilla-Cuesta, M. Skaf, A. Santamaría, J.J. Hernández-Bagaces, V. Ortega-López, Temporal flowability evolution of slag-based self-compacting concrete with recycled concrete aggregate, J. Clean. Prod. 299 (2021), 126890, https://doi.org/10.1016/j.jclepro.2021.126890.
[39] A. Santamaría, V. Ortega-López, M. Skaf, J.A. Chica, J.M. Manso, The study of properties and behavior of self compacting concrete containing Electric Arc Furnace Slag (EAFS) as aggregate, Ain Shams Eng. J. 11 (1) (2020) 231–243, https://doi.org/10.1016/j.asej.2019.10.001.
[40] British Standard Institution, BS-812: Testing Aggregates (1975).
[41] F. Faleschini, M. Alejandro Fernández-Ruíz, M.A. Zanini, K. Brunelli, C. Pellegrino, E. Hernández-Montes, High performance concrete with electric arc furnace slag as aggregate: Mechanical and durability properties, Constr. Build. Mater. 101 (2015) 113–121, https://doi.org/10.1016/j.conbuildmat.2015.10.022.
[42] M. Sigrüner, D. Muscat, N. Strübbe, Investigation on pull-out behavior and interface critical parameters of polymer fibers embedded in concrete and their correlation with particular fiber properties, J. Appl. Polym. Sci. 138 (28) (2021) 50745, https://doi.org/10.1002/app.50745.
[43] V. Ortega-López, J.A. Fuente-Alonso, A. Santamaría, J.T. San-José, Á. Aragón, Durability studies on fiber-reinforced EAF slag concrete for pavements, Constr. Build. Mater. 163 (2018) 471–481, https://doi.org/10.1016/j.conbuildmat.2017.12.121.
[44] A. Santamaría, A. Orbe, J.T. San José, J.J. González, A study on the durability of structural concrete incorporating electric steelmaking slags, Constr. Build. Mater. 161 (2018) 94–111, https://doi.org/10.1016/j.conbuildmat.2017.11.121.
[45] A. Santamaría, A. García-Llona, V. Revilla-Cuesta, I. Piñero, V. Ortega-López, Bending tests on building beams containing electric arc furnace slag and alternative binders and manufactured with energy-saving placement techniques, Structures 32 (2021) 1921–1933, https://doi.org/10.1016/j.istruc.2021.04.003.
[46] H. Qasrawi, Effect of the position of core on the strength of concrete of columns in existing structures, J. Build. Eng. 25 (2019), 100812, https://doi.org/10.1016/j.jobe.2019.100812.
[47] UNE CEN/TS 12390-9 EX, Testing hardened concrete. Part 9: Freeze-thaw resistance. Scaling (2008).
[48] ASTM-International, Book Annual of ASTM Standars, West Conshohocken, 19429–2959 2008 USA PA, (2008).
[49] S.I. Abu-Eishah, A.S. El-Dieb, M.S. Bedir, Performance of concrete mixtures made with electric arc furnace (EAF) steel slag aggregate produced in the Arabian Gulf region, Constr. Build. Mater. 34 (2012) 249–256, https://doi.org/10.1016/j.conbuildmat.2012.02.012.
[50] I.Z. Yildirim, M. Prezzi, Subgrade stabilisation mixtures with EAF steel slag: an experimental study followed by field implementation, Int. J. Pavement Eng. (2020) 10.1080/10298436.2020.1823389.
[51] V.M. Malhotra, Testing hardened concrete: nondestructive methods, Am. Concr. Inst. Monogr. 1975 (9) (1975).
[52] D. Karthik, K. Nirmalkumar, R. Priyadharshini, Characteristic assessment of self-compacting concrete with supplementary cementitious materials, Constr. Build. Mater. 297 (2021), 123845, https://doi.org/10.1016/j.conbuildmat.2021.123845.
[53] O.K. Djelloul, B. Menadi, G. Wardeh, S. Kenai, Performance of self-compacting concrete made with coarse and fine recycled concrete aggregates and ground granulated blast-furnace slag, Adv. Concr. Constr. 6 (2) (2018) 103-121. 10.12989/acc.2018.6.2.103.
[54] S.A. Santos, P.R. da Silva, J. de Brito, Mechanical performance evaluation of self-compacting concrete with fine and coarse recycled aggregates from the precast industry, Materials 10 (8) (2017) 904, https://doi.org/10.3390/ma10080904.
[55] M. Papachristoforou, E.K. Anastasiou, I. Papayianni, Durability of steel fiber reinforced concrete with coarse steel slag aggregates including performance at elevated temperatures, Constr. Build. Mater. 262 (2020), 120569, https://doi.org/10.1016/j.conbuildmat.2020.120569.
[56] J. Wang, Q. Dai, R. Si, Y. Ma, S. Guo, Fresh and mechanical performance and freeze-thaw durability of steel fiber-reinforced rubber self-compacting concrete (SRSCC), J. Clean. Prod. 277 (2020), 123180, https://doi.org/10.1016/j.jclepro.2020.123180.
[57] M. Benaicha, O. Jalbaud, A. Hafidi Alaoui, Y. Burtschell, Correlation between the mechanical behavior and the ultrasonic velocity of fiber-reinforced concrete, Constr. Build. Mater. 101 (2015) 702–709, https://doi.org/10.1016/j.conbuildmat.2015.10.047.
[58] A. Alzaza, K. Ohenoja, M. Illikainen, Enhancing the mechanical and durability properties of subzero-cured one-part alkali-activated blast furnace slag mortar by using submicron metallurgical residue as an additive, Cem. Concr. Compos. 122 (2021), 104128, https://doi.org/10.1016/j.cemconcomp.2021.104128.
[59] S.F. Selleck, E.N. Landis, M.L. Peterson, S.P. Shah, J.D. Achenbach, Ultrasonic investigation of concrete with distributed damage, ACI Mater. J. 95 (1) (1998) 27–36.
[60] M. Bagarić, I. Banjad Pečur, B. Milovanović, Hygrothermal performance of ventilated prefabricated sandwich wall panel from recycled construction and demolition waste – a case study, Energy Build. 206 (2020), 109573, https://doi.org/10.1016/j.enbuild.2019.109573.
[61] F. Fiol, C. Thomas, J.M. Manso, I. López, Influence of recycled precast concrete aggregate on durability of concrete's physical processes, Appl. Sci. 10 (20) (2020) 7348, https://doi.org/10.3390/app10207348.
[62] F. Bernachy-Barbe, T. Sayari, V. Dewynter-Marty, V. L'Hostis, Using X-ray microtomography to study the initiation of chloride-induced reinforcement corrosion in cracked concrete, Constr. Build. Mater. 259 (2020), 119574, https://doi.org/10.1016/j.conbuildmat.2020.119574.
[63] R. Choudhary, R. Gupta, T. Alomayri, A. Jain, R. Nagar, Permeation, corrosion, and drying shrinkage assessment of self-compacting high strength concrete comprising waste marble slurry and fly ash, with silica fume, Structures 33 (2021) 971–985, https://doi.org/10.1016/j.istruc.2021.05.008.
[64] L.V. Real, D.R.B. Oliveira, T. Soares, M.H.F. Medeiros, Silver nitrate spray colorimetric method for the evaluation of chloride penetration in concrete: state of the art, Revista ALCONPAT 5 (2) (2015) 151–161.
[65] J. Rosales, F. Agrela, J.A. Entrenas, M. Cabrera, Potential of stainless steel slag waste in manufacturing self-compacting concrete, Materials 13 (9) (2020) 2049, https://doi.org/10.3390/MA13092049.
[66] EC-2, Eurocode 2: Design of concrete structures. Part 1-1: General rules and rules for buildings, CEN (European Committee for Standardization) (2010).
[67] UNE 112011, Corrosion of concrete reinforcement steel. Determination of the carbonation depth for in-service concrete (2011).
[68] M.T. Blanco-Varela, J. Aguilera, S. Martínez-Ramírez, A. Palomo, C. Sabbioni, C. Riontino, G. Zappia, K. Vanvalen, E.E. Toumbakari, Thaumasite formation in hydraulic mortars by atmospheric SO2 deposition, Mater. Constr. 2001 (263–264) (2001) 109–125, https://doi.org/10.3989/mc.2001.v51.i263-264.357.